Assessing Target Specificity of the Small Molecule Inhibitor MARIMASTAT to Snake Venom Toxins: A Novel Application of Thermal Proteome Profiling

Authors

Cara F. Smith, Cassandra M. Modahl, David Ceja Galindo, Keira Y. Larson, Sean P. Maroney, Lilyrose Bahrabadi, Nicklaus P. Brandehoff, Blair W. Perry, Maxwell C. McCabe, Daniel Petras, Bruno Lomonte, Juan J. Calvete, Todd A. Castoe, Stephen P. Mackessy, Kirk C. Hansen, and Anthony J. Saviola

Correspondence

Anthony.Saviola@cuanschutz.edu

In Brief

Smith *et al.* investigate the utility of the proteome integral solubility alteration (PISA) assay for elucidating venom protein interactions with a small molecule inhibitor. Thermal proteome profiling experiments demonstrate that much of the Western Diamondback rattlesnake (Crotalus atrox) venom proteome is amenable to thermal denaturation. PISA identified specific SVMP proteoforms targeted by the matrix metalloprotease inhibitor marimastat, demonstrating that a PISA-based approach can provide rapid, highly sensitive, and robust inferences for the unbiased proteome-wide screening of venom and inhibitor interactions.

Graphical Abstract
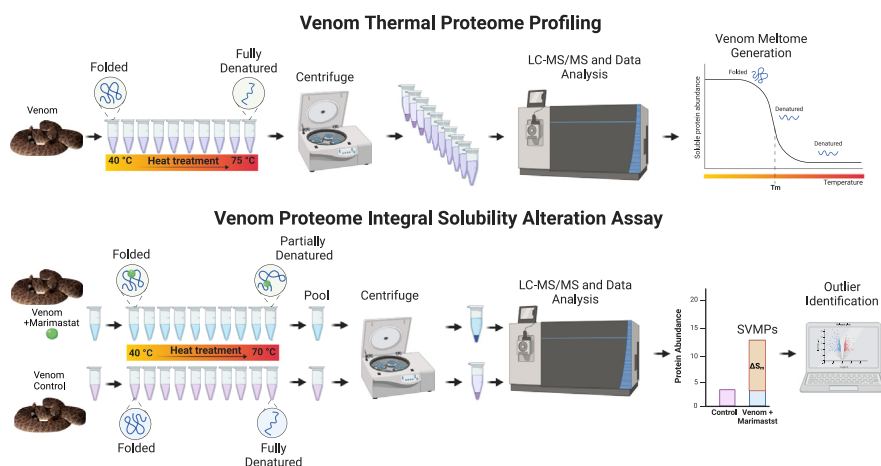
Highlights

- A significant proportion of the venom proteome is amenable to thermal denaturation.
- The PISA assay can identify venom protein targets of small molecule inhibitors.
- Both the supernatant and pellet provide useful and complementary information.
- Optimizing the thermal window based on the *Tm* of the target protein improves results.

Assessing Target Specificity of the Small Molecule Inhibitor MARIMASTAT to Snake Venom Toxins: A Novel Application of Thermal Proteome Profiling

Cara F. Smith[1], Cassandra M. Modahl[2], David Ceja Galindo[1], Keira Y. Larson[1], Sean P. Maroney[1], Lilyrose Bahrabadi[1], Nicklaus P. Brandehoff[3], Blair W. Perry[4], Maxwell C. McCabe[1], Daniel Petras[5,6], Bruno Lomonte[7], Juan J. Calvete[8], Todd A. Castoe[9], Stephen P. Mackessy[10], Kirk C. Hansen[1], and Anthony J. Saviola[1,*]

New treatments that circumvent the pitfalls of traditional antivenom therapies are critical to address the problem of snakebite globally. Numerous snake venom toxin inhibitors have shown promising cross-species neutralization of medically significant venom toxins *in vivo* and *in vitro*. The development of high-throughput approaches for the screening of such inhibitors could accelerate their identification, testing, and implementation and thus holds exciting potential for improving the treatments and outcomes of snakebite envenomation worldwide. Energetics-based proteomic approaches, including thermal proteome profiling and proteome integral solubility alteration (PISA) assays, represent "deep proteomics" methods for high throughput, proteome-wide identification of drug targets and ligands. In the following study, we apply thermal proteome profiling and PISA methods to characterize the interactions between venom toxin proteoforms in *Crotalus atrox* (Western Diamondback Rattlesnake) and the snake venom metalloprotease (SVMP) inhibitor marimastat. We investigate its venom proteome-wide effects and characterize its interactions with specific SVMP proteoforms, as well as its potential targeting of non-SVMP venom toxin families. We also compare the performance of PISA thermal window and soluble supernatant with insoluble precipitate using two inhibitor concentrations, providing the first demonstration of the utility of a sensitive high-throughput PISA-based approach to assess the direct targets of small molecule inhibitors for snake venom.

Snakebite is a global public health problem that disproportionately affects impoverished communities in rural tropical and subtropical regions. Annual estimates suggest that snakebite affects 1.8 to 2.7 million people worldwide, causing >138,000 deaths and leaving an even larger number of victims suffering permanent disabilities (1), which has led to the designation of snakebite as a neglected tropical disease by the World Health Organization (2, 3). Snake venoms are complex toxic cocktails of proteins and peptides derived from more than a dozen gene families, many of which have undergone duplication to generate multiple functionally diverse paralogs and associated proteoforms in the venom of a single species (4–6). While substantial variation exists in the relative mass and functional activity of venom proteins and peptides, most of these toxins have evolved to target and disrupt numerous bodily systems (7–10). Adding to the complexity of snake venoms, the most medically relevant toxin families tend to be the most diverse with many paralogs and associated proteoforms displaying moderate-to-high sequence similarity but in many cases exhibiting a spectrum of distinct biological effects (7, 9, 11–13). One of these families, snake venom metalloproteases (SVMPs), is ubiquitous across snake species (but is particularly abundant in viperid venoms) and is responsible for many of the life-threatening pathologies that result from snake envenomation, including local and systemic hemorrhage and tissue destruction (14–18).

From the [1]Department of Biochemistry and Molecular Genetics, University of Colorado Denver, Aurora, Colorado, USA; [2]Centre for Snakebite Research and Interventions, Liverpool School of Tropical Medicine, Liverpool, UK; [3]Rocky Mountain Poison and Drug Center, Denver Health and Hospital Authority, Denver, Colorado, USA; [4]School of Biological Sciences, Washington State University, Pullman, Washington, USA; [5]CMFI Cluster of Excellence, University of Tuebingen, Tuebingen, Germany; [6]Department of Biochemistry, University of California Riverside, Riverside, California, USA; [7]Instituto Clodomiro Picado, Facultad de Microbiología, Universidad de Costa Rica, San José, Costa Rica; [8]Evolutionary and Translational Venomics Laboratory, Consejo Superior de Investigaciones Científicas (CSIC), Valencia, Spain; [9]Department of Biology, The University of Texas Arlington, Texas, USA; [10]Department of Biological Sciences, University of Northern Colorado, Greeley, Colorado, USA

*For correspondence: Anthony J. Saviola, Anthony.Saviola@cuanschutz.edu.

The substantial morbidity and mortality resulting globally from snakebite may seem surprising considering that antivenoms (whole IgG molecules, Fab or F(ab′)$_2$ fragments from venom-immunized animals) are often highly effective at recognizing and neutralizing the major toxic components of a venom (19, 20). A major challenge to antivenom efficacy, however, is the significant variation in venom composition that occurs at phylogenetic (21–26), ontogenetic (27–30), and geographic or population scales (31–36). As a consequence, antivenoms are most effective against the snake species whose venom was utilized during production and are often inadequate at recognizing venom components of different or even closely related snake species (25). Further, geographic venom variation may even result in poor neutralization within the same species when snakes used in antivenom production were sourced from a different location (33). Antivenoms also tend to be more effective at neutralizing systemic effects but less effective at neutralizing anatomically localized manifestations of envenomation, which can result in permanent tissue damage and disfigurement (1, 37–41). The storage, accessibility, and administration of antivenom also pose significant practical challenges in rural areas where it is needed most (10, 37, 42–48). These hurdles are further compounded by the excessive effort and cost of producing antivenoms for any one geographically-relevant set of venomous snake species.

While the use of polyvalent antivenoms has been the mainstay treatment for snake envenomation, the development of non-immunological treatments that circumvent the limitations of antivenoms has been prioritized as a goal to address the impacts of snake envenomation globally by the World Health Organization (3). Recent applications of small molecule inhibitors against medically significant toxins have yielded promising preclinical results and these inhibitors have broad potential as supplemental therapies in combination with standard treatments (37, 49–54). These inhibitors have a number of advantages over current antivenom therapies including better peripheral tissue distribution, higher shelf stability, a higher safety profile, the ability for pre-hospital oral or topical administration, and greater affordability (55). The use of novel high-throughput approaches for the testing of venom toxin inhibitors and the identification of their targets could accelerate the implementation of effective small molecule inhibitors, with the long-term potential of improving the treatment and outcome of snakebite envenomation globally.

Numerous studies have examined the effects of various small molecule inhibitors on the biological activities of venoms *in vitro* and the neutralization capacity of these inhibitors *in vivo* (49–51, 53, 56–59). A repurposed low-specificity matrix metalloprotease inhibitor, marimastat, has shown effective neutralization of SVMP-rich venoms across multiple venomous snake species by preventing both local and systemic toxicity (53), decreasing hemotoxic venom effects (50, 51, 53, 60, 61), reducing SVMP-induced cytotoxicity (56, 60), and inhibiting extracellular matrix degradation (62). Because marimastat has previously progressed to clinical trials as a cancer treatment, its safety profile has already been determined, accelerating its development as a potential snakebite treatment (63, 64). When administered with other small molecule inhibitors, marimastat has shown *in vivo* neutralization of lethal toxicity and dermonecrosis in murine models (50, 56). Each of these studies assesses the downstream effects of inhibitor action *in vivo* or *in vitro* by measuring changes to biological activity or survival; however, to our knowledge, no studies exist using a direct assessment of venom-wide target–ligand interactions between venom toxins and small molecule inhibitors.

Thermal proteome profiling (TPP) is a prominent energetics-based proteomic approach for identifying the molecular targets of drugs. TPP builds upon the concept that a protein's physicochemical properties are altered through interactions with extrinsic factors (*e.g.*, other proteins, therapeutic drugs, metabolites) making it more or less resistant to thermal-induced denaturation (65, 66). Traditional TPP assays were centered on the principle that unbound proteins tend to denature and become insoluble when subjected to increasing temperatures, whereas proteins stabilized through interactions with extrinsic factors often exhibit increased thermal stability and remain in solution (65, 67–69). Identifying and quantifying such solubility changes *via* mass spectrometry can be used to infer direct or indirect interactions between a given compound and its protein targets (70).

Recently, the proteome integral solubility alteration (PISA) assay has emerged as a powerful strategy that retains the breadth and sensitivity of TPP but with a significant reduction in sample preparation and analysis time (70, 71). PISA represents a "deep proteomics" method for high throughput proteome-wide target identification of ligands, with improved target discovery and higher statistical significance for target candidates (70–72). In general, PISA experiments measure changes in protein precipitation that can be induced by altering temperature (70), solvent concentration (67), mechanical stress (73), or ion concentration (74). In a thermal PISA assay, samples are subjected to heat across a temperature gradient (as in TPP) but are subsequently pooled prior to analysis (70, 71). Rather than generating melt curves to determine exact melting temperatures, PISA compares overall abundance of each measured peptide between controls and treatments to detect differences in melting properties when a compound of interest is added. This methodology allows multiple variables to be altered simultaneously (*e.g.*, concentration, temperature) in a high-throughput manner. It has recently been shown that heat-treating within a smaller temperature window can improve sensitivity and target discovery with PISA (75). TPP, PISA, and related methods derived from the same principles have been used to discover drug targets, antibiotic targets, mechanisms of antibiotic resistance, and in the high-throughput screen of compound libraries (65, 66, 69, 76, 77). In our specific context, these proteomic techniques

applied to the development of envenomation treatments hold strong potential to provide rapid and high-throughput characterization of small molecule venom toxin inhibitors by determining their direct targets across diverse venom toxin protein families, accelerating identification of novel inhibitors.

Here, we apply TPP and PISA methods to characterize the physical interactions between the SVMP inhibitor marimastat and toxin proteoforms of *Crotalus atrox* (Western Diamondback Rattlesnake) venom. First, we determined toxin proteoform presence and abundance in the venom of this well-studied species and used TPP to characterize the venom meltome by determining venom protein family-level and specific proteoform-level thermal characteristics. Next, we performed PISA experiments within two different thermal windows to assess protein solubility changes upon inhibitor addition to identify specific proteoform targets of the small molecule inhibitor marimastat. Because of the previously characterized differences in signal-to-noise ratio between supernatant and pellet in PISA experiments (78, 79), we investigate and compare the targets identified in both the soluble and insoluble fractions. Our results demonstrate that a PISA-based approach can provide rapid, highly sensitive, and robust inferences for the unbiased proteome-wide screening of venom and inhibitor interactions.

EXPERIMENTAL PROCEDURES

Venom and Inhibitors

C. atrox (Western Diamondback rattlesnake) venom was obtained by manual extraction from snakes housed at the University of Northern Colorado (UNC) Animal Facility, in accordance with UNC-IACUC protocols. Venoms were lyophilized and stored at –20 °C until use. Venoms were reconstituted at a concentration of 2 mg/ml and protein concentration was determined on a Nanodrop using the Absorbance 280 program. The small molecule matrix metalloprotease inhibitor marimastat ((2*S*,3*R*)-*N*4-[(1*S*)-2,2-Dimethyl-1-[(methylamino)carbonyl] propyl]-*N*1,2-dihydroxy-3-(2-methylpropyl)butanediamide, >98%, Cat no.: 2631, Tocris Bioscience) was reconstituted in ddH$_2$0 at a concentration of 1.5 mM and stored at –20 °C.

Venom Gland Transcriptomics

An adult *C. atrox* (separate from those used for venom extraction) was collected in Portal, AZ under collecting permit 0456 and maintained in the UNC Animal Facility. Four days following manual venom extraction, the *C. atrox* was humanely euthanized and venom glands removed (IACUC protocol no. 9204). Approximately 70 mg of tissue, originating from both left and right venom glands, was homogenized. Total RNA was isolated from homogenized venom gland tissue using the previously described TRIzol (Life Technologies) protocol for venom glands (80, 81). A NEBNext Poly(A) mRNA magnetic isolation module (New England Biolabs) was used to select mRNA from 1 μg of total RNA, and the NEBNext Ultra RNA library prep kit (New England Biolabs) manufacture's protocol followed to prepare the sample for Illumina RNA-seq. During library preparation, products within the 200 to 400 bp size range were selected by solid phase reversible immobilization with the Agencourt AMPure XP reagent (Beckman Coulter) and PCR amplification consisted of 12 cycles. Final quantification of the RNA-seq library was done with the Library Quantification Kit for Illumina platforms (KAPA Biosystems). The *C. atrox* venom gland RNA-seq library was then checked for proper fragment size selection and quality on an Agilent 2100 Bioanalyzer, equally pooled with eight other unique barcoded RNA-seq libraries and sequenced on 1/8th of an Illumina HiSeq 2000 platform lane at the UC Denver Genomics core to obtain 125 bp paired-end reads.

To produce a comprehensive venom gland transcriptome database for *C. atrox*, two RNA-seq libraries were *de novo* assembled, the first from the *C. atrox* RNA-seq library detailed above and the second from a Texas locality *C. atrox* with reads available on the National Center for Biotechnology Information server (SRR3478367). Low quality reads were trimmed and adaptors removed using Trimmomatic (82) with a sliding window of four nucleotides and a threshold of phred 30. Reads were then assessed with FastQC (Babraham Institute Bioinformatics) to confirm that all adapters and low-quality reads were removed before *de novo* assembly. Three *de novo* assemblers were used in combination to produce a final, high-quality assembly: (i). first, a Trinity (release v2014-07-17) genome-guided assembly was completed using default parameters and Bowtie2 (v2.2.6) (83) aligned reads to the *C. atrox* genome (provided by Noah Dowell (84)), (ii) a second *de novo* assembly was completed with the program Extender (k-mer size 100) (85), performed with the same parameters as used for other snake venom glands (86) and with merged paired-end reads, merged with PEAR (Paired-End read mergeR v0.9.6; default parameters) (87), as seed and extension inputs, and (iii) a third *de novo* assembly was completed with VT Builder using default settings (88). From a concatenated fasta file of all three assemblies, coding contigs were then identified with EvidentialGene (downloaded May 2018) (89) and redundant coding contigs and those less than 150 bps were removed with CD-HIT (90, 91). Reads were aligned with Bowtie2 to coding contigs and abundances determined with RNA-seq by Expectation-Maximization (RSEM; v1.2.23) (92). Contigs less than 1 transcript per million were filtered out, and the remaining contigs annotated with Diamond (93) BLASTx (E-value 10^{-05} cut-off) searches against the NCBI non-redundant protein database. Transcripts were identified as venom proteins after each was manually examined to determine if the resulting protein was full-length, shared sequence identity to a currently known venom protein, and contained a shared signal peptide sequence with other venom proteins within that superfamily. This transcript set was also filtered through ToxCodAn (94) as a final toxin annotation check, and the resulting translated toxins used as a custom database for mass spectrometry. Sequenced reads are available under NCBI accession SRR26583170, bioproject PRJNA1033617. These sequences were combined with those utilized in Calvete *et al.*, (2009), and duplicate sequences removed.

Venom Meltome Generation

Thermal profiling assays were carried out following previously described methods (76, 95). Venom (1 μg/μl) was assayed in duplicate and divided into 10 aliquots of 20 μl and transferred to 0.2 ml PCR tubes. Each aliquot was individually heated at a single temperature over the range of 37 °C to 75 °C (37, 40, 45, 49, 52, 57, 62, 66, 69, 75 °C) for 3 min in a Bioer LifeECO thermal cycler (Fig. 1*A*). Samples were allowed to aggregate at 25 °C for 1 min and then placed on ice. Precipitated proteins were removed by centrifugation at 4 °C in 1.5 ml Eppendorf tubes (Thermo Fisher Scientific #3451) at 21,000*g* (14,000 RPM) for 45 min in an Eppendorf 5430 R centrifuge with an Eppendorf FA-45-30-11 rotor, and the supernatant was carefully removed with gel loading pipet tips (Fisher brand) and subjected to SDS-PAGE and sample preparation for mass spectrometric analysis.

Inhibitor PISA Assays

Venom (1 μg/μl) was incubated with two previously explored concentrations of marimastat, 15 μM or 150 μM (53, 61), or a vehicle
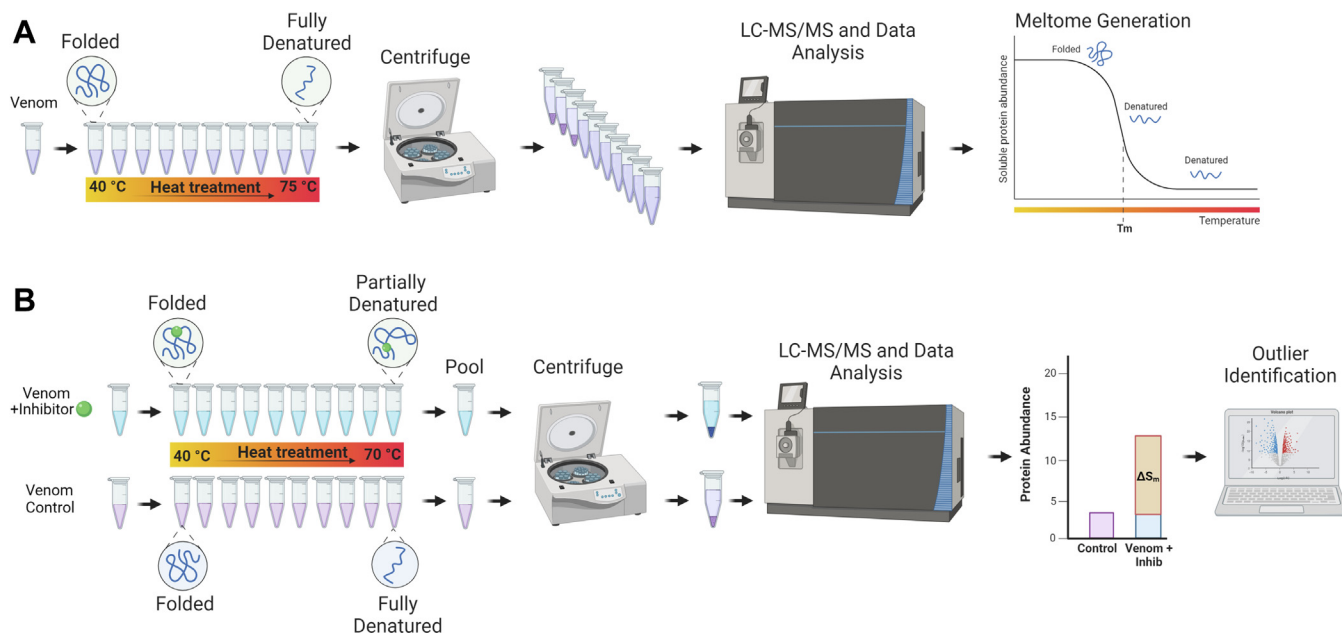
Fig. 1. **TPP and PISA workflows.** *A*, in TPP experiments, samples are heated between 40–70 °C and centrifuged to pellet denatured proteins. Samples are reduced, alkylated, and trypsin digested and analyzed with LC-MS/MS for protein identification. Melting curves are generated in ProSAP using unique intensity for each protein identified. T_m = melting temperature of 50% of population. *B*, in PISA, venom is incubated for 30 min at 37 °C with an inhibitor or alone. Samples are heated from 40 to 70 °C and pooled before centrifuging to pellet insoluble material. Samples are prepared as mentioned above and analyzed *via* LC-MS/MS for protein identification. To identify inhibitor targets, unique intensity is used to calculate SAR values for each protein followed by identification of significant outliers. PISA, proteome integral solubility alteration; TPP, thermal proteome profiling.

control (ddH$_2$O) for 30 min at 37 °C. Each sample was then divided into 12 aliquots of 20 μl in 0.2 ml PCR tubes. Each aliquot was individually heated at a different temperature from 40 °C to 70 °C for 3 min in a Bioer LifeECO Thermal cycler (Fig. 1*B*), allowed to cool at 25 °C for 1 min, and placed on ice. An equal volume of sample from each temperature point was pooled and centrifuged at 21,000*g* for 45 min at 4 °C to separate the soluble fraction from insoluble denatured proteins (70).

Previous PISA performance assessment has demonstrated higher sensitivity in the precipitated fraction which showed a greater fold change in abundance compared to supernatant (Peng *et al.*, 2016). Because of these previously characterized differences in performance between supernatant and pellet, we investigated both fractions (78, 79). The volume corresponding to 30 μg of soluble protein (based on controls) was taken from all samples (65) and prepared for mass spectrometry and 20 μg was used for gel electrophoresis. PISA assays for each condition were performed in triplicate. Because selection of a narrower temperature window for heat denaturation has been shown to increase sensitivity of the PISA assay (75), we also performed a temperature gradient denaturation with five temperatures (selected based on SVMP family-level T_m values) from 56 °C to 60 °C. Samples were pooled and processed as described above.

High-Performance Liquid Chromatography

One mg of venom incubated with either 150 μM marimastat or a vehicle control (ddH$_2$O) was subjected to reverse phase high-performance liquid chromatography (HPLC) after heat treatment using a Waters system, Empower software, and a Phenomenex Jupiter C$_{18}$ (250 × 4.6 mm, 5 μm, 300 Å pore size) column as outlined in Smith and Mackessy (96). Proteins/peptides were detected at 280 nm and 220 nm with a Waters 2487 Dual λ Absorbance Detector. Fractions corresponding to each peak were collected and then frozen at −80 °C

overnight, lyophilized, and then separated with SDS-PAGE as previously described (96). Percent peak area and peak height at 280 nm were recorded as a proxy for relative toxin abundance.

Sodium Dodecyl Sulfate Polyacrylamide Gel Electrophoresis

SDS-PAGE materials were obtained from Life Technologies, Inc (Grand Island). DTT-reduced venom (20 μg) or lyophilized protein (approximately 5 μg—reverse-phase high-performance liquid chromatography (RP-HPLC) fractionated) was loaded into wells of a NuPAGE Novex Bis-Tris 12% acrylamide Mini Gel and electrophoresed in MES buffer under reducing conditions for 45 min at 175 V; 7 μl of Mark 12 standards were loaded for molecular weight estimates. Gels were stained overnight with gentle shaking in 0.1% Coomassie brilliant blue R-250 in 50% methanol and 20% acetic acid (v/v) and destained in 30% methanol, 7% glacial acetic acid (v/v) in water until background was sufficiently destained (approximately 2 h). Gels were then placed in storage solution (7% acetic acid, v/v) for several hours with gentle shaking at room temperature and imaged on an HP Scanjet 4570c scanner. Protein families were identified based on previously published reports and electrophoretic patterns for numerous rattlesnake venoms and several purified venom enzymes (97–99).

Sample Preparation for Liquid Chromatography-Tandem Mass Spectrometry

The volume of supernatant corresponding to 30 μg of venom proteins in the non-heat denatured control was dried in a vacuum centrifuge and redissolved in 8 M urea/0.1 M Tris (pH 8.5) and reduced with 5 mM tris (2-carboxyethyl) phosphine for 20 min at room temperature. Samples were then alkylated with 50 mM 2-chloroacetamide for 15 min in the dark at room temperature, diluted 4-fold with 100 mM Tris–HCl (pH 8.5), and trypsin digested at an enzyme/substrate ratio of

1:20 overnight at 37 °C. To stop the reaction, samples were acidified with formic acid (FA), and digested peptides were purified with Pierce C18 Spin Tips (Thermo Fisher Scientific #84850) according to the manufacturer's protocol. Samples were dried in a vacuum centrifuge and redissolved in 0.1% FA.

Electrophoretic protein bands subjected to liquid chromatography-tandem mass spectrometry (LC-MS/MS) were excised from Coomassie-stained gels, destained, and subjected to in-gel reduction, alkylation, and overnight trypsin digestion as previously described (100). Following the overnight digestion, samples were acidified with 5% FA and tryptic peptides were extracted in 30 µl of 50% acetonitrile/1% FA. Digests were dried in a vacuum centrifuge and redissolved in 0.1% FA for mass spectrometry.

Nano Liquid Chromatography Tandem Mass Spectrometry

Nano liquid chromatography tandem mass spectrometry was performed using an Easy nLC 1000 instrument coupled with a Q-Exactive HF Mass Spectrometer (both from ThermoFisher Scientific). Approximately 3 µg of digested peptides were loaded on a C_{18} column (100 µm inner diameter × 20 cm) packed in-house with 2.7 µm Cortecs C_{18} resin and separated at a flow rate of 0.4 µl/min with solution A (0.1% FA) and solution B (0.1% FA in ACN) under the following conditions: isocratic at 4% B for 3 min, followed by 4 to 32% B for 102 min, 32 to 55% B for 5 min, 55 to 95% B for 1 min and isocratic at 95% B for 9 min. Mass spectrometry was performed in data-dependent acquisition mode. Full MS scans were obtained from m/z 300 to 1800 at a resolution of 60,000, an automatic gain control target of 1×10^6, and a maximum injection time of 50 ms. The top 15 most abundant ions with an intensity threshold of 9.1×10^3 were selected for MS/MS acquisition at a 15,000 resolution, 1×10^5 automatic gain control, and a maximal injection time of 110 ms. The isolation window was set to 2.0 m/z and ions were fragmented at a normalized collision energy of 30. Dynamic exclusion was set to 20 s.

Analysis of Mass Spectrometry Data

Fragmentation spectra were interpreted against a custom protein sequence database, comprising 570 entries generated from the assembly of *C. atrox* venom gland transcriptome data (described above) combined with UniProt entries of all toxins found in the *C. atrox* venom proteome (97), reverse decoys and contaminants, and using MSFragger v3.8 within the FragPipe (v20.0) computational platform (101, 102). Cysteine carbamidomethylation was selected as a fixed modification, oxidation of methionine was selected as a variable modification, and precursor-ion mass tolerance and fragment-ion mass tolerance were set at 20 ppm and 0.4 Da, respectively. Fully tryptic peptides with a maximum of two missed tryptic cleavages were allowed and the protein-level and peptide-level false discovery rate was set to <1%. The relative abundance of major snake venom toxin families was compared across samples using sum-normalized total spectral intensity (103).

Analysis of TPP Data

Protein melting curves were generated by fitting sigmoidal curves to relative protein abundances using the Protein Stability Analysis Pod (ProSAP) package (104). The temperature at which relative protein abundance reached 50%, T_m (melting temperature), was determined in ProSAP by normalizing intensity to the lowest temperature (37 °C), followed by normalization to the most thermostable proteins as previously described (79). Duplicates were averaged to determine the average T_m of all identified venom toxins. Venom proteins failing to reach 50% denaturation even at higher temperatures were classified as non-melting proteins.

Analysis of PISA Data

PISA data was analyzed as previously described (71, 103). Briefly, PISA uses the ΔS_m value or soluble abundance ratio (SAR) as opposed to the T_m to determine differences in thermal stability (70). ΔS_m represents the difference in integral abundance of a protein in treated compared to untreated samples. We performed a two-tailed Student's *t* test with unequal variance to calculate *p*-values ($p < 0.05$). Changes to venom protein abundance were visualized using volcano plots based on $\log_2$SAR values and $-\log_{10}$ transformed *p*-values. Proteins with a $\log_2$SAR value ≥ 0.5 or ≤ -0.5 and a $-\log_{10}$ transformed *p*-value ≥ 1.3 ($p < 0.05$) were identified as toxins with a significant shift in solubility. All figures were made with BioRender.com.

RESULTS

C. atrox *Venom Proteome*

Previous characterization of the *C. atrox* venom proteome revealed the presence of at least 24 proteins belonging to eight different venom toxin protein families (Fig. 2A; (97)) and, more recently, the presence of 31 SVMP genes in *C. atrox* with 15 to 16 expressed SVMPs (105). SVMPs and snake venom serine proteases (SVSPs) were the two most abundant protein families representing nearly 70% of the venom proteome. L-amino acid oxidase (L-AAO), phospholipase A_2 (PLA$_2$), disintegrins, and cysteine-rich secretory proteins (CRISPs) comprise most of the remaining 25% of *C. atrox* venom proteins, whereas vasoactive peptides, endogenous SVMP inhibitors, and C-type lectins (CTLs) comprised the remaining small fraction of venom components comprising <2% of the venom proteome. Utilizing the protein database generated from protein sequences of proteins identified by Calvete *et al.* (97) combined with protein sequences derived from a *C. atrox* venom gland transcriptome, we detected 46 unique proteoforms with at least one unique peptide in *C. atrox* venom (Fig. 2B). Venom toxins with the highest number of distinct proteoforms detected included 13 CTLs, 13 SVMPs, nine SVSPs, and three PLA$_2$s (Fig. 2B). We identified only one unique proteoform of more abundant proteins including L-AAO and CRISP and only one proteoform for minor components bradykinin-potentiating peptide (BPP), glutaminyl-peptide cyclotransferase, hyaluronidase, nerve growth factor, phospholipase B, and vascular endothelial growth factor (VEGF).

RP-HPLC analysis revealed a complex toxin profile of *C. atrox* venom similar to that of Calvete *et al.*, 2009 (Fig. 2C). We used SDS-PAGE of peak fractions (Supplemental Fig. S1) combined with the peak elution times and identified masses in Calvete *et al.* (97) to confirm peak identities. BPP's eluted between 8 and 15 min with co-elution of disintegrins and SVMP inhibitors. PLA$_2$ eluted at 27, 30, and between 39 to 44 min, CRISP eluted at 29 min, SVSP eluted between 32 to 36 min, L-AAO eluted at 46 min, and SVMPs eluted between 51 to 56 min (Fig. 2C).

C. atrox *Venom Meltome*

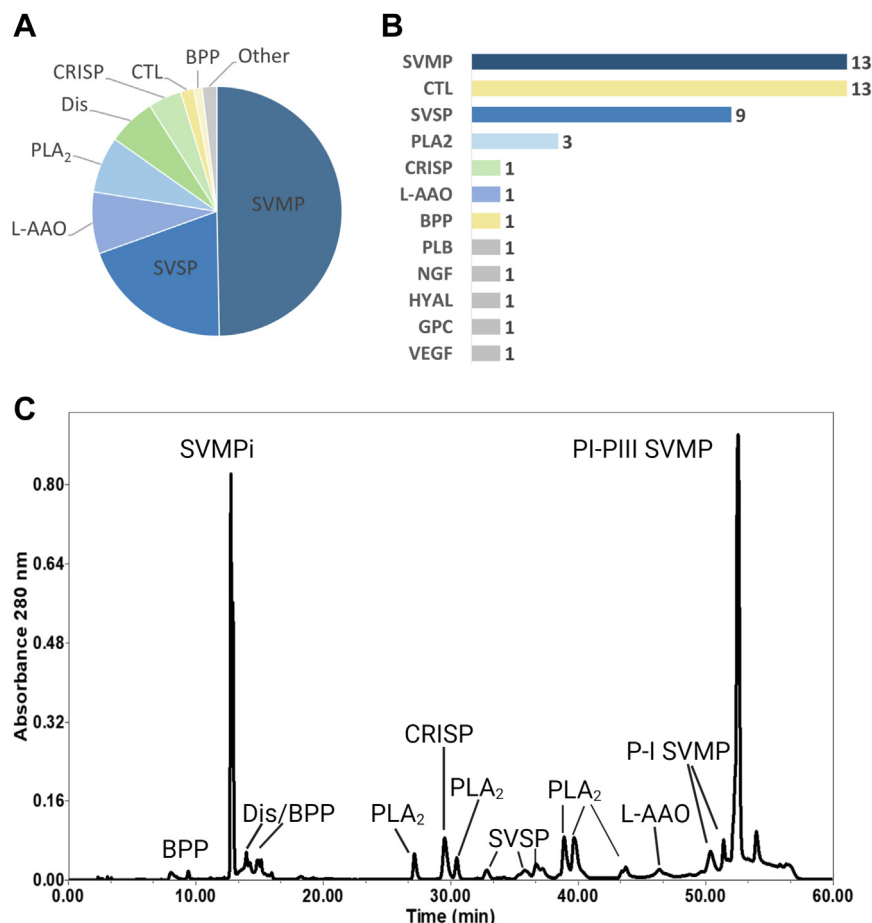With the goal of demonstrating the utility of applying a PISA workflow for identifying venom protein interactions with

FIG. 2. ***Crotalus atrox* venom proteome characterization.** *A*, toxin family abundances in *C. atrox* venom modified from Calvete *et al.*, 2009. *B*, the number of proteoforms identified in *C. atrox* venom in the present study organized by family. *C*, RP-HPLC separated *C. atrox* venom. For peak identification, fractions were analyzed with mass spectrometry and SDS-PAGE and compared to known masses from Calvete *et al.*, 2009. PP, bradykinin potentiating peptide; CRISP, cysteine rich secretory protein; CTL, C-type lectin; Dis, disintegrin; GPC, glutaminyl-peptide cyclotransferase; HPLC, high-performance liquid chromatography; HYAL, hyaluronidase; L-AAO, L-amino acid oxidase; NGF, nerve growth factor; PLA_2, phospholipase A_2; PLB, phospholipase B; RP-HPLC, reverse-phase high-performance liquid chromatography; SVMP, snake venom metalloprotease; SVMPi, SVMP tripeptide inhibitor; SVSP, snake venom serine protease; VEGF, vascular endothelial growth factor.

a small molecule inhibitor, we first assessed the effects of thermal stress on the venom proteome. Venom was subjected to increasing temperatures ranging from 40 to 75 °C, allowed to cool at room temperature, followed by separation and removal of aggregates from each temperature point by centrifugation. The soluble fractions were then visualized by gel electrophoresis (Fig. 3A) and prepared for LC-MS/MS. SDS-PAGE analyses of these fractions indicate that the entire venom proteome appeared to exhibit some degree of denaturation between the temperatures tested with clear differences in denaturation observed across venom protein families (Fig. 3A). For example, L-AAO, hyaluronidase, SVMPs, and CTLs appeared more thermally sensitive while SVSP, CRISP, PLA_2, and disintegrin families exhibited greater stability at higher temperatures.

Next, we assessed the thermal stability of venom proteins across the ten different temperature points by LC-MS/MS.

An equal volume of each soluble fraction was collected and subjected to reduction, alkylation, trypsin digestion, and LC-MS/MS. Fragmentation spectra were interpreted against our *C. atrox*–specific custom venom proteome sequence database, and we used the ProSAP package (104) to determine melting points for each venom protein family. When normalized to thermostable proteins, most venom proteins show decreasing abundance with increasing temperature, with the majority of proteins reduced in abundance at temperatures above 62 °C (Fig. 3B). The distribution of toxin melting temperature (T_m) values ranged from 47.8 to 74.3 °C (Fig. 3, C and D; Supplemental Table S1). Most toxins had T_m's between 50 to 60 °C (Fig. 3D; n = 22) or 60 to 70 °C (n = 28), and only 11 proteoforms were still thermostable with no calculable T_m at 75 °C (BIP, BPP, VEGF, 4 PIII-SVMPs, and 4 SVSPs; Fig. 3D). The five toxins with the lowest T_m's included four CTLs (average T_m = 49.3 °C,
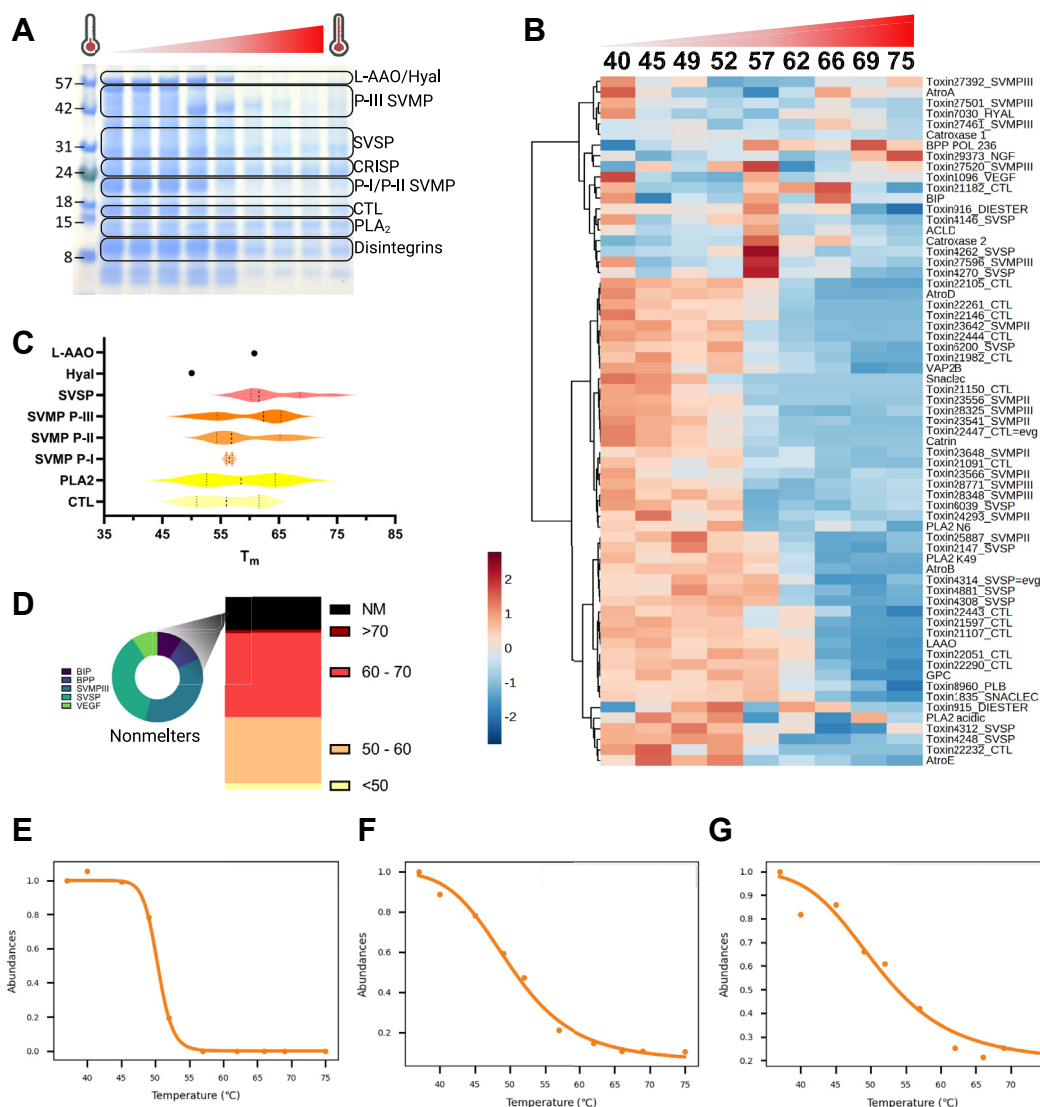
FIG. 3. **Crotalus atrox** meltome characterization. *A*, SDS-PAGE of *C. atrox* venom heated at temperatures between 37–70 °C for 3 min. *B*, heatmap showing the soluble fraction of most toxin proteoforms relative to 37 °C in *C. atrox* venom at 40, 45, 49, 52, 57, 62, 66, 69, and 75 °C. Heatmap colors represent the number of SDs away from the mean of the protein's intensity in each row of the heatmap. *C*, distribution of melting temperatures organized by family. *Dotted lines* represent median and quartile ranges. *D*, distribution of melting temperatures for all toxins identified. Nonmelters (NM) are classified as proteoforms for which T_m could not be calculated when heated to a maximum temperature of 75 °C. *E*, representative melting curve of a CTL (Crotocetin). Abundance is normalized to 37 °C. *F*, representative melting curve of a PLA$_2$ (Cvv-N6). Abundance is normalized to 37 °C. *G*, representative melting curve of an SVMP (PIII 28325). Abundance is normalized to 37 °C. CTL, c-type lectin; SVMP, snake venom metalloprotease.

stdev = 1.1 °C; Fig. 3, *C* and *E*) and the single hyaluronidase proteoform (T_m = 50.6 °C). CTLs T_m values as a whole ranged from 47.8 to 63.1 °C (ave = 56.0 °C, stdev = 5.3 °C). PLA$_2$s had an average T_m of 61.2 °C (stdev = 8.3 °C; Fig. 3, *C* and *F*). The different SVMP subfamilies differed slightly in their melting range but were not significantly different (p = 0.77; Fig. 3*C*). PI-SVMP proteoforms had an average T_m of 56.8 °C (stdev = 0.03 °C), PIIs averaged 59.3 °C (stdev = 5.7 °C; Fig. 3*C*), and PIII's averaged 59.7 °C (stdev = 6 °C; Fig. 3*G*). SVSPs had the highest average T_m (63.9 °C, stdev = 5.5 °C) and made up a large proportion of the

proteins that were thermostable above 75 °C (Fig. 3*B*). The single L-AAO proteoform identified melted at 61.7 °C. In general, melting temperatures were reproducible between replicates with an average SD of 1.17 °C between replicates. These results demonstrate protein family-level differences in thermal stability, in that all proteoforms of some families denatured (*i.e.*, CTL, SVMP I) when subjected to heat, while others appear resistant to thermal perturbation (SVSPs). These results indicate that a significant proportion of the venom proteome is amenable to thermal denaturation.

Venom-Wide Interactions with Marimastat

After establishing that venom proteins are susceptible to thermal denaturation, we next assessed if a PISA strategy could be applied to elucidate small molecule-venom protein engagement. For this, we applied the PISA assay, an approach where samples across the entire temperature gradient of the same treatment are pooled prior to preparation and mass spectrometric analysis (66, 70, 71). With traditional PISA, the abundance of the protein(s) in the soluble fractions of the pooled samples is then used to assess the effect of a compound on its solubility (70). For highly thermostable proteins, monitoring supernatant alone is likely not effective in thermal-shift–based methods (79). Because increases in protein solubility upon compound binding also result in decreased protein abundance within the precipitated pellet, quantifying protein abundance in the precipitate pellet can also identify protein targets (79). Further, because of different observed signal-to-noise ratios, soluble and pelleted materials may perform differently in PISA assays to identify significant thermal shifts (78, 79). Utilizing precipitated material to measure changes in protein solubility can additionally reduce the

false discovery rate and improve sensitivity of the assay. Based on this logic, we utilized both supernatant and precipitated material to investigate the effects of marimastat.

PISA assays were performed on marimastat, an inhibitor of matrix metalloproteases that has shown significant inhibitory activity against SVMPs (50, 51, 53, 56, 60–62). *C. atrox* venom was incubated with marimastat (15 μM and 150 μM) or vehicle (ddH$_2$O) for 30 min at 37 °C. Following incubation, each sample was divided into 12 aliquots and subjected to increasing temperatures from 40 to 70 °C. Equal aliquots per temperature point were then pooled, protein aggregates were separated by centrifugation, and the soluble and insoluble fractions of the vehicle and inhibitor-treated venoms were prepared for downstream analysis.

When filtering criteria were applied ($p < 0.05$, and log$_2$-SAR>0.5), the lower concentration of marimastat (15 μM) caused five of 21 SVMP proteoforms (PIII 28348, PIII 28325, PII 25887, PII 23541, and VAP 1) to display a stabilizing shift in treated supernatant compared to untreated supernatant (Fig. 4A). In addition to these five proteoforms, two additional
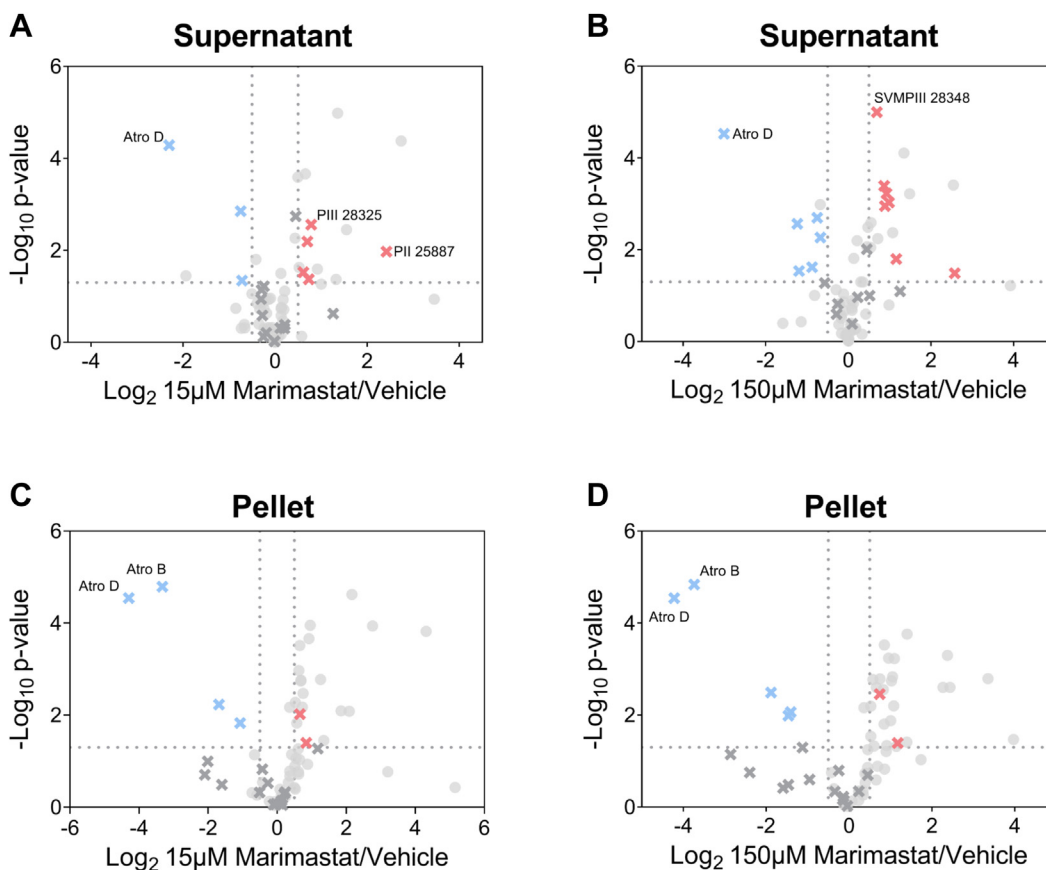

FIG. 4. ***Crotalus atrox*** **venom-wide interactions with two concentrations of marimastat with temperature window from 40 to 70 °C.** *A*, volcano plot comparing soluble supernatant of heat-treated venom + marimastat (15 μM) to heat-treated venom alone. X indicates SVMP proteoforms, *red* = positive outliers, *blue* = negative outliers, *gray* = not significant. *B*, volcano plot comparing soluble supernatant of heat-treated venom + marimastat (150 μM) to heat-treated venom alone. *C*, volcano plot comparing insoluble precipitate of heat-treated venom + marimastat (15 μM) to heat-treated venom alone. *D*, volcano plot comparing insoluble precipitate of heat-treated venom + marimastat (150 μM) to heat-treated venom alone. SVMP, snake venom metalloprotease.

SVMPs (PII 23556 and PII 27392) were more abundant in the supernatant of venom treated with 150 μM of marimastat (Fig. 4B; Supplemental Table S2).

Next, we compared the pellets of untreated venom to venom treated with both concentrations of marimastat. When filtering criteria were applied at the low concentration, only four SVMPs (Atro B, Atro-D, SVMPIII 27520, and SVMPIII 28348) were detected at significantly lower abundance in the treated pellet than the control pellet, indicative of a stabilizing effect of marimastat (Fig. 4C). These same proteoforms, in addition to SVMP PII 23541, were also significantly reduced in the pellet of the higher marimastat concentration (Fig. 4D). The presence of positive outliers identified in both the supernatant and negative outliers in the precipitate of treated venom indicates an overall stabilizing effect of marimastat on venom targets.

Validation of Inhibitor Interactions

To validate our PISA results showing the stabilizing effects of marimastat on SVMPs, we performed SDS-PAGE and RP-HPLC on non-heat-denatured venom and venoms treated with marimastat or vehicle. The toxin family composition of the peaks and bands altered by the addition of marimastat was confirmed by mass spectrometry (Supplemental Tables S3 and S4). In the heated marimastat-treated venom, gel bands A and B were composed predominantly of PIII 27501 and VAP2B (band A) and PII 23556, Atro E and Atro B (band B; Fig. 5A). Band C was composed of acidic PLA$_2$, band D of PLA2 Cax-K49, CTL 22443, and PLA2 Cvv-N6, and band E was predominantly CTL 21182, CTL 22444, and PLA2 Cax-K49. SDS-PAGE analysis of the heat-denatured and undenatured control venom shows a clear reduction in the size and intensity of SVMP-PIII (~50 kDa; band A), SVMP P-I/II (~20 kDa; band B), and CTL/PLA$_2$ gel bands (~10–14 kDa; bands C-E) in response to thermal treatment (Fig. 5A). This reduction in SVMP and CTL/PLA$_2$ band size and intensity in response to heat appears to be partially to fully recovered when venom is incubated with 150 μM marimastat (Fig. 5A).

RP-HPLC peaks eluting between 51 to 54 min were identified by mass spectrometry as SVMPs, with VAP2B, PIII 27501, P-III ACLD, PII 23556, PIII 28348, PII 23566, and Atro E representing the dominant proteoforms (Fig. 5B). These
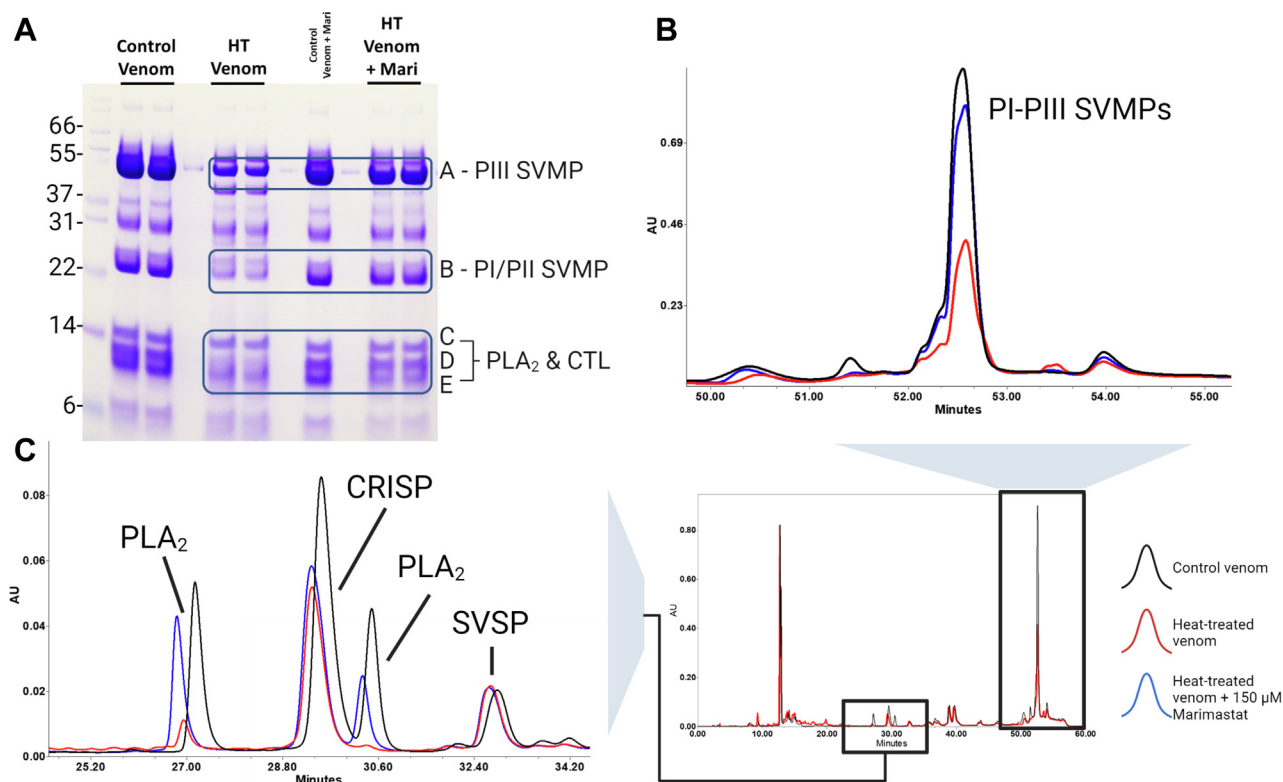

FIG. 5. **Validation assays of inhibitor interactions.** *A*, SDS-PAGE comparison of heat-treated venom to heat-treated venoms incubated with 150 μM of marimastat with a thermal window of 40–70 °C. Note the recovery in band size and intensity of SVMP and PLA$_2$ bands in marimastat-treated samples. The *left* side indicates molecular mass standards in kDa. *B*, enlarged HPLC-separated SVMP peak overlay comparing abundance of non-heat-treated venom (*black*), heat-treated venom (*red*), and venom heat-treated after incubation with 150 μM of marimastat (*blue*). Note the recovery of peak area in the inhibitor-treated sample. *C*, enlarged HPLC-separated PLA$_2$ peak overlay comparing abundance of non-heat-treated venom (*black*), heat-treated venom (*red*), and venom heat-treated after incubation with 150 μM of marimastat (*blue*). Note the recovery of PLA$_2$ peak area in the inhibitor-treated sample. HPLC, high-performance liquid chromatography; SVMP, snake venom metalloprotease.

continued to be the dominant proteoforms with the exception of Atro E in both the heated control and marimastat-treated venoms. The 27-min, 29-min, and 30-min peaks were composed predominantly of the basic PLA_2 Cax-K49, CRISP, and basic PLA_2 Cvv-N6, respectively (Fig. 5C). These remained the dominant proteoforms in the heated control venom and marimastat-treated venom, with the exception of marimastat-treated peak 30 where CRISP became the dominant proteoform followed by PLA_2 Cvv-N6.

The stabilizing effect of marimastat on some venom proteins is further demonstrated by the analysis of RP-HPLC, which shows partial recovery in the chromatographic peak area and peak height of SVMP and two PLA_2 peaks in the marimastat-treated venoms compared to the controls (Fig. 5, B and C). After heat treatment, SVMPs lose 44% of their original peak area, but marimastat treatment results in only a 7% decrease in peak area after melting (Fig. 5B). The PLA_2 proteins eluting at 27 min decreases by 75% when venom is heat-treated and only 26% when venom is treated with marimastat, while the PLA_2 eluting at 30 min is virtually absent in the heated control venom but only loses 52% abundance when heat-treated with marimastat (Fig. 5C). Peak heights of PLA_2 (27 min), PLA_2 (30 min), and SVMPs decrease by 81%, 100%, and 57% respectively after melting; however, with marimastat, peak height only decreases by 21%, 48%, and 21%, respectively (Fig. 5, B and C).

VAP2B is the dominant proteoform in *C. atrox* venom (Fig. 5B; Supplemental Tables S3 and S4) and was the second most abundant proteoform in the SVMP fractions and gel bands of treated venom. However, it was not detected as a stabilized outlier in either supernatant or pellet in the current PISA experiments performed with the temperate range of 40 to 70 °C. Thus, we aimed to increase the sensitivity of the PISA assay with a narrower thermal window determined by the T_m values previously calculated for the target toxin family.

Venom-Wide Interactions with Marimastat in a Narrowed Thermal Window PISA

While PISA is advantageous because it reduces the analysis time and sample preparation while still being effective at target discovery, it may sacrifice sensitivity compared to TPP experiments due to the pooling of all temperature points, and melting temperature selection can have a drastic effect on thermal behavior in PISA experiments (75, 79). To investigate this, we compared the performance of a broad thermal window (40–70 °C) to a narrower window (56–60 °C), selected based on the mean and SD of T_m's of SVMPs, the target venom toxin family. We performed PISA assays with the same concentrations of marimastat, with a narrower temperature window from 56 to 60 °C with five temperature points of each sample replicate, which has been shown to improve the overall sensitivity of the PISA assay in target identification (75).

When samples were heat treated with a narrower window of temperatures, the lower concentration of marimastat

displayed three of 21 SVMP proteoforms (PIII 28348, PIII 28325, PII 23541) at a greater abundance in treated supernatant than untreated supernatant (Fig. 6A; Supplemental Table S4). At the higher concentration, seven of 21 proteoforms were higher in supernatant of treated venom: VAP1, PIII 28348, PIII 28325, PII 23556, PII 23541, PIII 28771, PIII 27392 (Fig. 6B). In the pellets of samples treated with a narrower range of temperatures, 11 of 21 proteoforms (VAP2B, PIII 28348, Atro D, PIII 27501, PII 23541, Atro B, PIII 27461, PIII 27520, PIII 28771, PII 23648, PIII 27392) demonstrated an increase in solubility in the pellet of the lower concentration of marimastat condition (Fig. 6C). These same proteoforms plus PII 23556 were reduced in the pellet at the higher concentration of marimastat (Fig. 6D).

Heat-Treatment Comparison

Next, we compared the performance of a broad thermal window (40–70 °C) and a narrower thermal window (56–60 °C) to the results gathered from our validation experiments (Figs. 4–6). At both temperature ranges when venom was treated with marimastat, principal component analysis shows clustering of the replicates based on treatment condition, with the two marimastat-treated groups separating from the vehicle-treated samples (Fig. 7, A–D). These results indicate that both concentrations of marimastat interact with venom protein targets and alter the solubility of venom proteins compared to the control group. However, pellet replicates (Fig. 7, B and D) cluster more tightly together in both conditions than in supernatants with greater separation among the treatment groups (Fig. 7, A and C). The highest amount of variance explained (97%) by the top two principal components was in the narrow window pellet, though all plots had a high percentage of sample variance explained (>86%). The number of significantly stabilized proteins found in the supernatant ($p < 0.05$, $log_2SAR \geq 0.5$) after treatment with marimastat at a broad melting window were 12 and 14 for 15 μM and 150 μM, respectively (Fig. 7E). The percentage of SVMPs among the identified proteins was 42% and 50%. At the narrower melting window, four and nine proteins were identified in 15 μM and 150 μM treatments, respectively, but SVMPs comprised 75% and 78% of identified proteins. In general, pellets of both melting windows appeared to perform better regardless of concentration. The precipitated pellet from 150 μM-treated venom heated at the narrower thermal window identified the most SVMP proteoforms of any treatment group. Though the broader temperature window precipitate identified fewer SVMP proteoforms, SVMPs were the only venom toxin family proteoforms identified, while the supernatant appeared to contain more, potentially off-target, non-SVMP identifications. The broad melting window identified four and five SVMP proteoforms, while the narrow window pellets identified 11 and 12 for 15 μM and 150 μM, respectively (Fig. 7E).

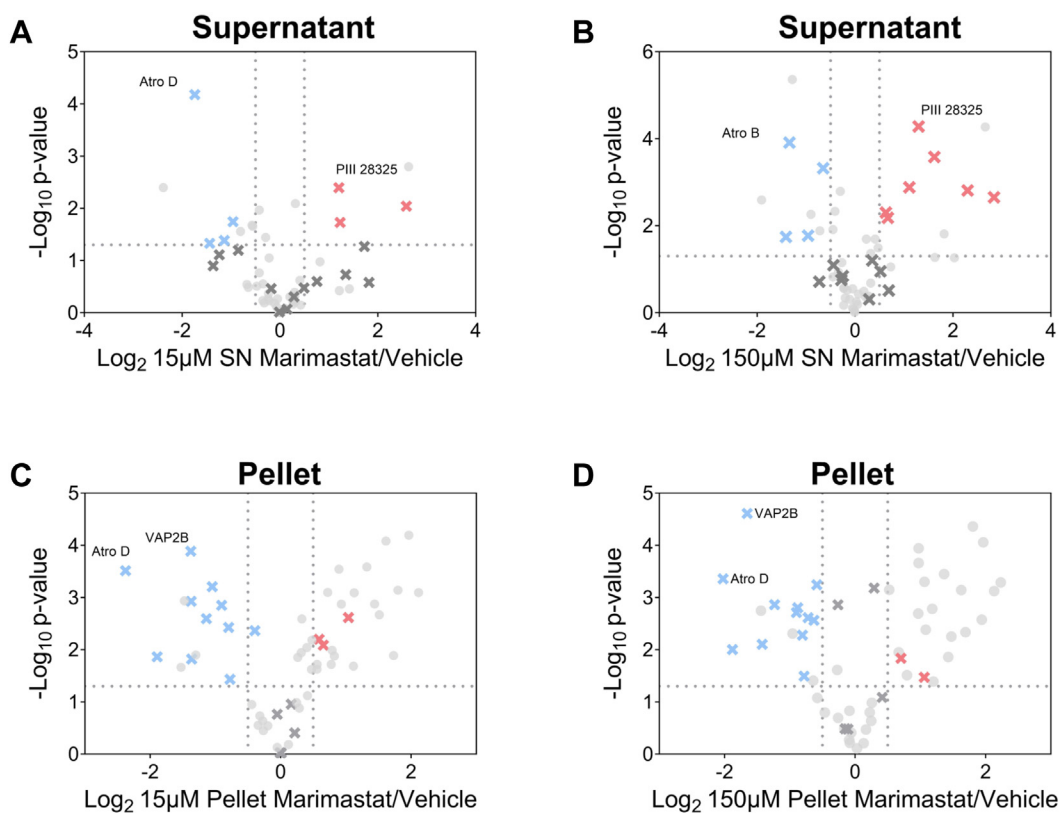Performance of specific SVMP proteoform identification between melting windows varied significantly at both

FIG. 6. ***Crotalus atrox* venom-wide interactions with two concentrations of marimastat with temperature window from 56 to 60 °C.** *A*, volcano plot comparing soluble supernatant of heat-treated venom + marimastat (15 μM) to heat-treated venom alone. X indicates SVMP proteoforms, *red* = positive outliers, *blue* = negative outliers, *gray* = not significant. *B*, volcano plot comparing soluble supernatant of heat-treated venom + marimastat (150 μM) to heat-treated venom alone. *C*, volcano plot comparing insoluble precipitate of heat-treated venom + marimastat (15 μM) to heat-treated venom alone. *D*, volcano plot comparing insoluble precipitate of heat-treated venom + marimastat (150 μM) to heat-treated venom alone. SVMP, snake venom metalloprotease.

concentrations, with only one common proteoform at 15 μM (Fig. 7*F*) and two at 150 μM (Fig. 7*G*). At both concentrations, the narrow window pellets had the highest number of uniquely identified SVMP proteoforms. When soluble abundance ratios (log$_2$SAR) of supernatant and pellets are compared, the narrower thermal window performs significantly better at identifying the target and off-target proteoforms that meet significance criteria in both supernatant and pellet. When only proteins meeting significance criteria for both supernatant and pellet were compared, the broad window performed poorly, identifying only two SVMPs (PIII 28348, PII 23541) with significant stabilizing shifts (Fig. 7*H*). The narrower window identified six SVMP proteoforms with significant stabilizing shifts (VAP1, PII 23556, PIII 28348, PIII 28771, PII 23541, PIII 27392) (Fig. 7*I*). Off-target proteins that met significance criteria for both conditions included hyaluronidase and, using the narrower window, three SVSPs and VEGF.

Coefficients of Variance

To determine consistency of label-free quantification measurements and ensure that observed alterations are reliable,

coefficients of variance (CVs) were calculated for each venom protein across the different replicates in each group. These individual protein CVs were then averaged to determine the mean variance for each analysis group. In general, CVs were low across replicate groups, with an average intra-group CV of 17.2% for all venom proteins, including all analysis groups and both narrow and wide melt range data. Average intra-group CVs were lowest for the high marimastat supernatant (10.33%), high marimastat pellet (10.68%), and low marimastat pellet (13.69%) groups. Average CVs were greater for the low marimastat supernatant (26.61%), control supernatant (18.57%), and control pellet (23.33%) groups. However, all comparisons used to draw conclusions maintain significance despite this variability.

SVMP Comparisons and Target Identification

Because the narrower temperature window appears to identify more target proteoforms with less noise, we utilized this narrow window approach to re-analyze interactions between SVMPs and marimastat. More SVMP proteoforms were identified as significant with a narrower window when
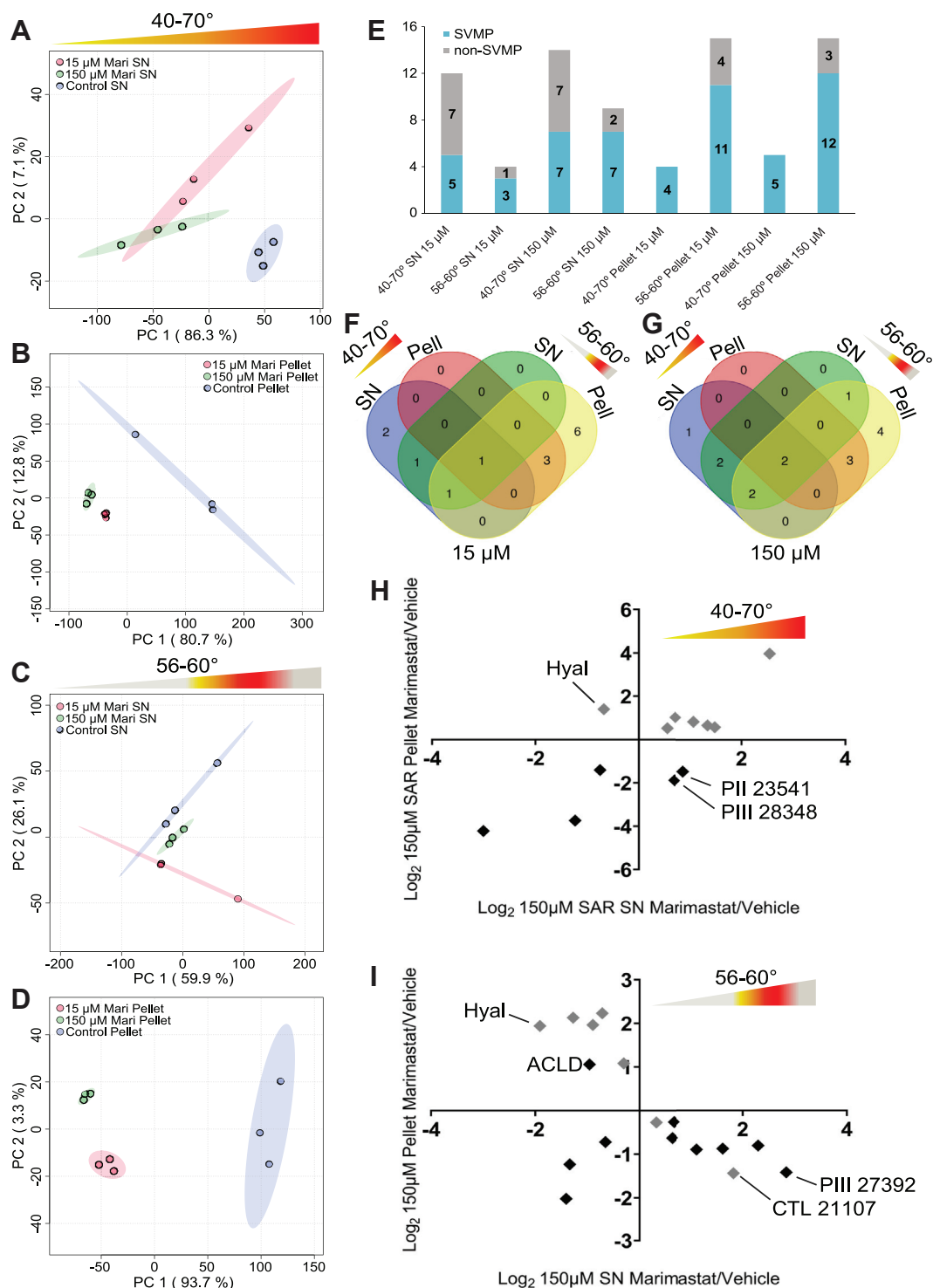
FIG. 7. **Comparison of a broad (40–70 °C) to a narrow (56–60 °C) PISA thermal window.** PCA plot comparing replicates of soluble supernatant of (A) heat-treated venom + 15 μM marimastat to heat-treated venom alone and (B) heat-treated venom +150 μM marimastat to heat-treated venom alone. PCA plot with 95% confidence intervals comparing replicates of insoluble precipitate of (C) heat-treated venom +15 μM marimastat to heat-treated venom alone and (D) heat-treated venom +150 μM marimastat to heat-treated venom alone. E, number of SVMP and non-SVMP proteins identified with significant thermal shifts toward stabilization (p-value < 0.05 log$_2$SAR> 0.5) after 15 μM or 150 μM marimastat treatment in supernatants and pellets heat-treated at a broad (40–70 °C) or a narrow (56–60 °C) thermal window. Venn diagrams of SVMP proteins identified with significant thermal shifts toward stabilization (p-value < 0.05, log$_2$SAR > 0.5) in supernatants and pellets heat-treated at a broad (40–70 °C) or a narrow (56–60 °C) thermal window after (F) 15 μM or (G) 150 μM marimastat treatment. Scatter plot showing log$_2$SAR

analyses of the supernatant and pellet were combined (Fig. 7, *E–G*), and analyses of the pellet identified more SVMP proteoforms than the supernatant within the narrower thermal window (Fig. 8*A*). Specifically, analysis of the narrow-range pellet identified highly abundant proteins also identified in the validation assays but not identified using the broad thermal window (*e.g.*, VAP2B). Hierarchical clustering analysis comparing supernatants and pellets at both concentrations shows an inverse relationship between relative intensity of each proteoform in the pellet *versus* the supernatant (Fig. 8*B*). When these conditions are compared to controls, we resolved three patterns of various proteoforms: (1) proteoforms that showed a positive shift (trend towards stabilization) in the supernatant at both concentrations of marimastat; (2) proteoforms that disappear from the pellet after marimastat treatment but do not necessarily increase in SAR in the supernatant (trend towards stabilization); and (3) proteoforms that increase in pellet SAR after treatment (Fig. 8*C*). Finally, correlation analysis performed with the SAR values of proteoforms supernatants and pellets of the narrow thermal window identified three clusters of proteoforms with similar shifts in thermal behavior: (1) a cluster containing the proteoforms that were stabilized by marimastat (*e.g.*, VAP2B, 27501, 23556, 27392) that represent the strongest targets of marimastat, (2) a cluster containing atrolysin B, atrolysin D, and PIII 27520 which appeared to decrease in abundance in both supernatants and pellets after marimastat treatment, and (3) a cluster that did not appear to be thermally stabilized by marimastat including atrolysin A, PII 24293 (Fig. 8*D*). The strongest target list includes proteoforms identified in the validation protein gel (*e.g.*, VAP2B, PIII 27501, PII 23556, PIII 28348, PIII 27392, and PII 23648) and those identified as most abundant in the SVMP HPLC peaks (VAP2B, PIII 27501, PII 23556, PIII 28348, PIII 27461).

While the most abundant proteoforms were identified as significant in analysis of the pellet but not in the corresponding supernatant, there does appear to be more noise in the pellet data indicated by the number of non-target proteins that reached significance with a $p < 0.05$, $log_2SAR \geq 0.5$ (upright right quadrants; Figs. 4, *C* and *D* and 6, *C* and *D*). This could be due to differences in solubilization of proteins in the pellet indicating that the soluble fraction analysis is more reliable in quantification. However, to examine the validity of analyzing the pellet for identifying high abundance targets, we use VAP2B as an example. In the case of VAP2B, the stabilizing effect of marimastat is only evident in the pellet, and both 15 μM and 150 μM concentrations have significantly lower levels of the precipitated toxin ($p = 0.003$, $p = 0.0013$, respectively, Fig. 8*E*). A less abundant proteoform, PIII 28348,

showed an increase in solubility that was detected in both the pellet and the supernatant at both concentrations of marimastat (Fig. 8*F*). In the pellet, abundance of PIII 28348 was significantly lower at both concentrations than in the untreated control ($p = 0.0004$, $p = 0.0014$, respectively) and significantly higher in the supernatant compared to control ($p < 0.0001$).

Off-Target Effects

Based on recovery of peak area in PLA_2 and CTL-containing peaks and gel bands in marimastat-treated venom subjected to RP-HPLC (Fig. 5*C*), we explored the possibility of using PISA assays to detect off-target effects of marimastat. Interestingly, at both concentrations with the wider thermal window, we observed changes in thermal behavior indicative of a shift towards stabilization of some non-target protein families, including two PLA_2 proteoforms (Cax-K49 and Cvv-N6) and four CTL proteoforms. In the gels, there was recovery of band E containing Cax-K49 and CTL's 22443, 21182, and 22444. Both PLA_2 proteoforms were repeated positive outliers in supernatants of all conditions but were not significant in any pellets. Various CTL proteoforms including CTL 21107, 22105, 22447, 21150, and 22232 were significant outliers in some conditions. When comparing only significant log_2SAR values in both supernatant and pellet, hyaluronidase, VEGF, two SVSPs, and two CTL's (22444, 21107) were significantly correlated between pellet and supernatant at the narrower melt window (Fig. 7*I*).

DISCUSSION

The development and testing of alternative snakebite therapeutics that are affordable, stable, and easily administered is an urgent global need (1, 10, 47, 106). Small molecule inhibitors currently lead the field of possible supplementary snake envenomation therapies, with phase II clinical trials ongoing for the PLA_2 inhibitor varespladib (107) and the SVMP inhibitor DMPS ((108); ClinicalTrials.gov, 2021). Numerous inhibitors have shown promising cross-species efficacy *in vivo* and *in vitro* (37, 50, 53, 57, 109), indicating that they may be less vulnerable to the effects of venom variation than traditional antibody-based antivenoms. However, additional preclinical studies are needed to evaluate the neutralizing efficacy and specificity of these drugs alone and in combination, and the development of these drugs would be accelerated by implementation of high throughput screening of interactions and efficacy across many species. Research on small molecule inhibitors of snake venom toxins has typically focused on *in vitro* and *in vivo* functional assays based on the known or likely biological activities of toxins (49–53, 58, 109–113). These

---

values calculated from 150 μM marimastat-treated venom *versus* vehicle treatment heated at from (*H*) 40–70 °C or (*I*) 56 to 60 °C that meet significance criteria in both supernatant (SN) and precipitate (Pellet) group. Largest outliers of SVMP and non-SVMP proteoforms are labeled. ACLD, PIII SVMP ACLD; *black*, SVMP proteoforms; Con, control; CTL, C-type lectin; *gray*, non-SVMP toxins; Hyal, hyaluronidase; PCA, principal component analysis; Pell, pellet; PISA, proteome integral solubility alteration; SN, supernatant; SVMP, snake venom metalloprotease.
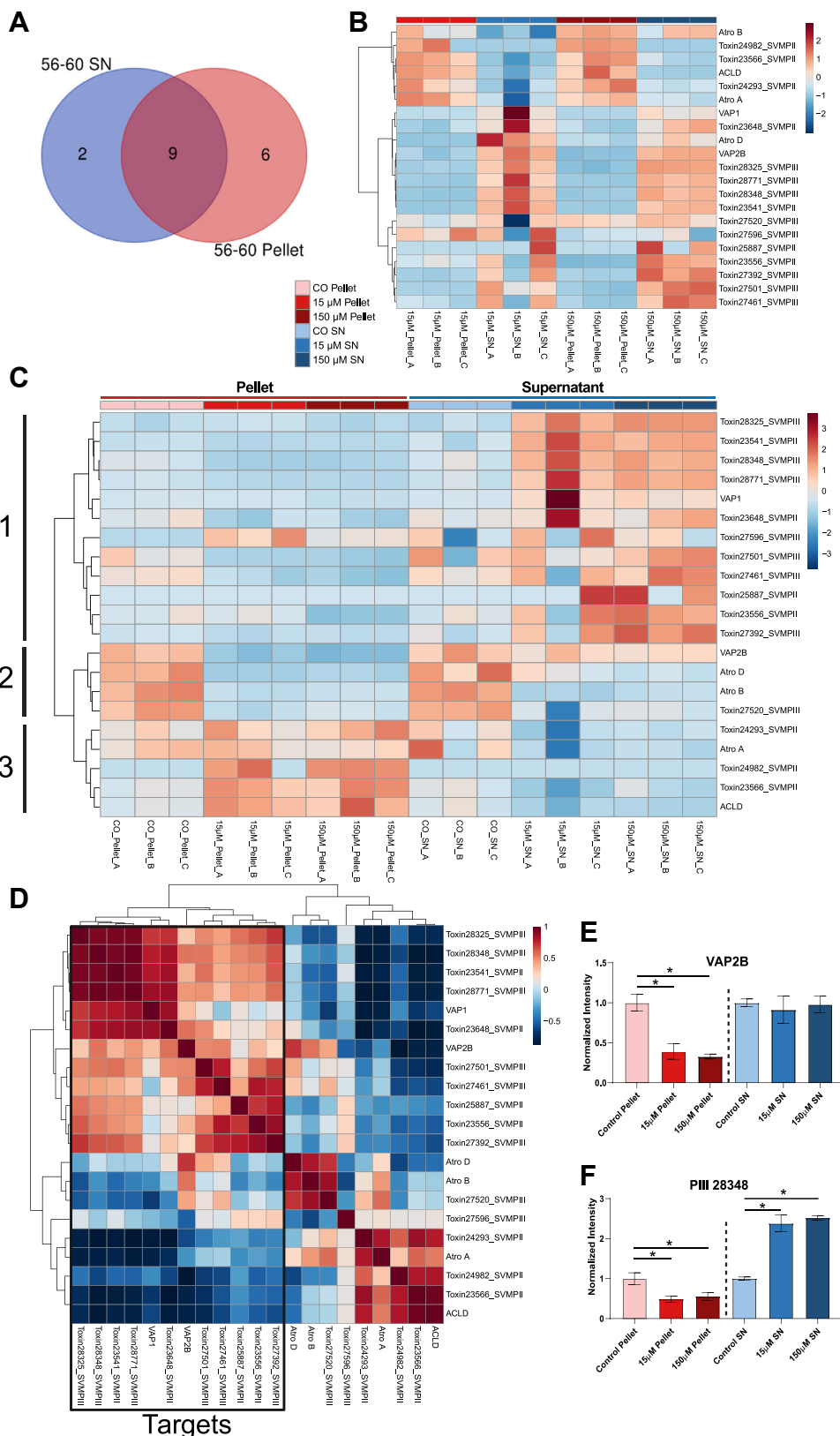
FIG. 8. **Effects of marimastat treatment and a narrow thermal window on SVMP proteoforms only.** *A*, number of proteins identified in supernatant (SN) and pellet of narrow thermal window that meet significance criteria (*p*-value < 0.01, $\log_2$SAR> 0.5); (*B*) heatmap of sum-normalized intensity values in supernatant or precipitate of SVMPs from 15 μM or 150 μM marimastat-treated venom. Heatmap colors are

approaches utilize a downstream measurement of the presumed interactions of an inhibitor with its targets (ex. reduced specific activity or increased survival). A previous study performed molecular docking analysis using marimastat and a purified PI SVMP proteoform CAMP-2 to demonstrate a direct interaction (51). However, the PISA method outlined here represents both a direct and venom-wide assessment of target-ligand engagement and provides the opportunity to link direct target–ligand interactions with functional and phenotypic responses (71, 72, 114).

In this study, we investigate the thermal characteristics of the *C. atrox* venom proteome and use this to develop a PISA-based assessment of the venom proteome-wide targets of the SVMP inhibitor marimastat. We investigate both its proteome-wide effects and determine and validate its interactions with specific venom proteoforms of its target toxin family (SVMPs) as well as possible off-target protein families. We identified a suite of marimastat proteoform-level targets and confirmed them by RP-HPLC and SDS-PAGE. We also compared the performance of soluble supernatant and insoluble precipitate at two different inhibitor concentrations for target identification. Our results provide a promising first assessment of the application of a PISA-based approach as a sensitive and high-throughput method to assess the direct targets of small molecule inhibitors for snake venom. Based on our experiments with PISA in this context, we find that analysis of the insoluble fraction from venom that was treated with a high concentration of marimastat, but a narrow thermal window for PISA, provided more sensitive target data with the least noise than other tested methods.

Previous research has shown that small molecule inhibitor efficacy *in vitro* may not always translate to *in vivo* efficacy. For example, the SVMP inhibitor prinomastat and the metal chelator dimercaprol showed moderate to high SVMP inhibitory activity *in vitro* but failed to confer any protection towards crude venom in *in vivo* assays (60). Furthermore, studies have highlighted cross-species variation in neutralization effects of potential inhibitors, which has significant implications for the application of inhibitors as broadly effective pre-hospital treatments of envenomation by potentially diverse species (58). Dimercaprol showed promise in murine models as an SVMP inhibitor against *Echis ocellatus* venom (115); however, it lacked this protective effect *in vivo* against *Dispholidus typus* venom (60), likely due to the high levels of divergence in venom composition between these distantly related species. While some inhibitors have demonstrated neutralization

capacity of specific biological effects (such as anticoagulation) caused by venoms of divergent species, they may vary in effectiveness across species because of lineage-specific variation in venom toxin sequence, activity, or relative abundance or because the same biological effects may arise due to the action of different toxin families altogether (58, 60). Knowledge of the snake species-specific venom-wide and proteoform-specific efficacy of inhibitors has the potential to significantly improve our ability to predict cross-species neutralization and to unravel the disparity between *in vitro* and *in vivo* results.

Before PISA could be widely applied for the screening of a large number of potential inhibitors against snake venom, a number of considerations must be addressed. By pooling a wide range of temperature points, PISA data in particular may suffer from reduced screening sensitivity, depending on the specific thermal properties of various proteins (75). Venom toxins appear to have significantly higher T_m values than human cell types, which ranged from 48 to 52 °C (95). Some potential snake venom toxin families of interest (*i.e.*, SVSPs and CRISPs) display high thermal tolerance likely due to increased frequency of disulfide bonds and other post-translational modifications, such as sulfation, glycosylation, and amidation, among others (116). Further, these properties and amino acid differences between proteins of the same family (117) may stabilize proteins at intermediate states during thermal stress to prevent irreversible denaturation resulting in proteins that refold partially back to their original states (118). Therefore, a thermal shift assay would be less than ideal to investigate inhibitor–toxin interactions for such thermo-stable proteoforms. However, thermal-based target deconvolution studies are still suitable for a wide range of unique systems including the study of venom metalloproteins in the presence of chelating agents, for example, DMPS and dimercaprol, both of which have demonstrated therapeutic potential towards treating snakebite (49, 115). For example, it was recently demonstrated that TPP with chelating agents can be used to identify novel metal-binding proteins (74). Based on the target family-level thermal properties determined by TPP, we refined our PISA assay parameters to a more sensitive thermal window for target identification and showed that a narrower thermal window selection can improve inhibitor target identification. These findings highlight how knowledge of general thermal properties of a toxin family of interest might be used to improve target identification, perhaps even for protein families with higher thermal stability.

scaled by row to better visualize variation in sum-normalized intensity between classes. *C*, heatmap of sum-normalized intensity values in supernatant or precipitate of SVMPs from 15 μM or 150 μM marimastat-treated venom or vehicle control showing concentration-dependent shifts in abundance. Heatmap colors are scaled by row to better visualize variation in sum-normalized intensity between classes. *D*, correlation plot of SAR values showing strongest marimastat targets based on the effects of marimastat treatment on SVMP proteoform intensity. Comparison of concentration-dependent intensity shifts between precipitate and supernatant of (*E*) the most abundant SVMP proteoform VAP2B and (*F*) a less abundant SVMP proteoform PIII 28348 at both concentrations of marimastat at the narrow thermal window. SVMP, snake venom metalloprotease.

Our results demonstrate how analysis of the composition of both supernatants and pellets can be complementary and thus be integrated to further refine inferences of molecular targets (78, 79). In our experiments, we observed varying performances between supernatant and pellet data in the consistent identification of inhibitor targets, particularly of the high abundance SVMP proteoform VAP2B. We found that precipitated material of the narrowed thermal window provided enhanced sensitivity for target deconvolution of the most abundant toxins and across the proteome in general. As previously noted, precipitated material produces better signal-to-noise ratios and more apparent stability ratios than analysis of supernatant (78). Indeed, some previously investigated well-known drug targets were only identified in the precipitated material, with no corresponding stability ratio shift in the supernatant (78), as seen with VAP2B in our study. These findings indicate that pelleted material is not just complementary to supernatant-based results but may also be critical for thorough target deconvolution. This is likely due to the continued presence of many proteins even at high temperatures as observed in this study and in previous studies (78). We also noted differing performances of the two tested marimastat concentrations on target identification, where the higher concentration provided both a higher number of possible SVMP targets and less noise than the lower concentration of marimastat.

In addition to providing information about direct target interactions, PISA also allows for off-target effects to be investigated. Off-target binding of a drug may result in adverse effects that decrease (or complicate) its therapeutic utility (114, 119), and small molecule drugs in particular tend to bind a myriad of molecular targets (120). For example, inhibitors of serine proteases exist that may be effective against medically significant SVSPs, but they may also cross-react with endogenous serine proteases in human plasma, which are critical for normal coagulation cascade activation (58). Our PISA analyses identified evidence of the putative interactions between marimastat and off-target toxin families, including CTLs and PLA_2 toxins, which were also supported by our liquid chromatography and gel electrophoresis results. These findings are also consistent with prior studies that have shown marimastat and another SVMP inhibitor, prinomastat, can reduce PLA_2-based anticoagulant venom effects (54). CTLs have been shown to complex with SVMPs (121), suggesting that there could be a stabilizing effect in conjunction with SVMPs. PLA_2s are medically significant enzymes that tend to be fairly ubiquitous and abundant across diverse snake venoms (24, 122–124). Though we did not detect any reduction in PLA_2 activity in marimastat-treated samples (data not shown), off-target effects should be considered when investigating small molecule inhibitors of snake venom toxins, as they may demonstrate effects on other medically significant targets and/or contribute to unexpected outcomes *in vivo*.

Multiple snake venom gene families have undergone substantial gene family expansion, diversification, and neofunctionalization that has in many cases resulted in elevated rates of nonsynonymous substitutions in regions of these proteins that determine biological function (12). This trend has been observed in SVMPs (125), SVSPs (126), PLA_2s (127, 128), and 3FTXs (129) and has resulted in large multi-gene toxin families with similar structure but a wide array of biological functions and pharmacological effects which can also vary substantially across species (5, 9, 11, 13, 130). Indeed, this diversity of proteoforms within and across species presents an extreme challenge for the development of effective therapeutics to target the effects of these diverse and species-specific toxin cocktails. A major step to addressing this challenge has resulted in efforts to identify the most bioactive and medically relevant toxic proteins and proteoforms in venom using "omics" technologies, which have been referred to as "toxicovenomics" (131–134). A PISA-based approach in combination with toxicovenomics has the potential to take the key next step to address this complex problem through the screening of molecules that may neutralize the action of venom toxins across a wide variety of species that display high variability of medically significant venom toxin families, proteoforms, and activities. PISA and other high-throughput approaches provide promising paths forward for screening of large numbers of commonly studied and currently unexplored inhibitors against a wide scope of venoms for more rapid development of alternative snakebite therapies.

DATA AVAILABILITY

The mass spectrometry proteomics data have been deposited to the ProteomeXchange Consortium *via* the PRIDE partner repository with the dataset identifier PXD046399.

Stephen P. Mackessy, and A. J. S. visualization; C. F. S., C. M. M., B. L., T. A. C., Stephen P. Mackessy, K. C. H., and A. J. S. writing–original draft; C. F. S., C. M. M., B. W. P., M. C. M., D. P., B. L., J. J. C., T. A. C., Stephen P. Mackessy, K. C. H., and A. J. S. writing–review and editing; A. J. S. supervision.

Conflict of interest—The authors declare that they have no conflicts of interests with the contents of this article.

Abbreviations—The abbreviations used are: BPP, bradykinin-potentiating peptide; CRISP, cysteine-rich secretory protein; CTL, C-type lectin; CV, coefficient of variance; FA, formic acid; HPLC, high-performance liquid chromatography; L-AAO, L-amino acid oxidase; LC-MS/MS, liquid chromatography-tandem mass spectrometry; PISA, proteome integral solubility alteration; ProSAP, Protein Stability Analysis Pod; RP-HPLC, reverse-phase high-performance liquid chromatography; SAR, soluble abundance ratio; SVMP, snake venom metalloprotease; SVSP, snake venom serine protease; TPP, thermal proteome profiling; UNC, University of Northern Colorado; VEGF, vascular endothelial growth factor.

REFERENCES

1. Gutiérrez, J. M., Calvete, J. J., Habib, A. G., Harrison, R. A., Williams, D. J., and Warrell, D. A. (2017) Snakebite envenoming. *Nat. Rev. Dis. Primers* **3**, 17063
2. Chippaux, J. P. (2017) Snakebite envenomation turns again into a neglected tropical disease. *J. Venom. Anim. Toxins Incl. Trop. Dis.* **23**, 1–2
3. Minghui, R., Malecela, M. N., Cooke, E., and Abela-Ridder, B. (2019) WHO's Snakebite Envenoming Strategy for prevention and control. *Lancet Glob. Health* **7**, e837–e838
4. Casewell, N. R., Wagstaff, S. C., Harrison, R. A., Renjifo, C., and Wüster, W. (2011) Domain loss facilitates accelerated evolution and neofunctionalization of duplicate snake venom metalloproteinase toxin genes. *Mol. Biol. Evol.* **28**, 2637–2649
5. Casewell, N. R. (2017) Evolution: gene Co-option Underpins venom protein evolution. *Curr. Biol.* **27**, R647–R649
6. Hargreaves, A. D., Swain, M. T., Hegarty, M. J., Logan, D. W., and Mulley, J. F. (2014) Restriction and recruitment-gene duplication and the origin and evolution of snake venom toxins. *Genome Biol. Evol.* **6**, 2088–2095
7. Casewell, N. R., Wüster, W., Vonk, F. J., Harrison, R. A., and Fry, B. G. (2013) Complex cocktails: the evolutionary novelty of venoms. *Trends Ecol. Evol.* **28**, 219–229
8. Vonk, F. J., Casewell, N. R., Henkel, C. V., Heimberg, A. M., Jansen, H. J., McCleary, R. J. R., *et al.* (2013) The king cobra genome reveals dynamic gene evolution and adaptation in the snake venom system. *Proc. Natl. Acad. Sci. U. S. A.* **110**, 20651–20656
9. Casewell, N. R., Huttley, G. A., and Wüster, W. (2012) Dynamic evolution of venom proteins in squamate reptiles. *Nat. Commun.* **3**, 1066
10. Williams, D. J., Gutiérrez, J. M., Calvete, J. J., Wüster, W., Ratanabanangkoon, K., Paiva, O., *et al.* (2011) Ending the drought: new strategies for improving the flow of affordable, effective antivenoms in Asia and Africa. *J. Proteomics* **74**, 1735–1767
11. Casewell, N. R., Wagstaff, S. C., Wuster, W., Cook, D. A. N., Bolton, F. M. S., King, S. I., *et al.* (2014) Medically important differences in snake venom composition are dictated by distinct postgenomic mechanisms. *Proc. Natl. Acad. Sci. U. S. A.* **111**, 9205–9210
12. Sunagar, K., Jackson, T. N. W., Undheim, E. A. B., Ali, S. A., Antunes, A., and Fry, B. G. (2013) Three-fingered RAVERs: rapid Accumulation of variations in Exposed Residues of snake venom toxins. *Toxins (Basel).* **5**, 2172–2208
13. Brust, A., Sunagar, K., Undheim, E. A. B., Vetter, I., Yang, D. C., Casewell, N. R., *et al.* (2013) Differential evolution and neofunctionalization of snake venom metalloprotease domains. *Mol. Cell. Proteomics* **12**, 651–663
14. Olaoba, O. T., Karina dos Santos, P., Selistre-de-Araujo, H. S., and Ferreira de Souza, D. H. (2020) Snake venom metalloproteinases (SVMPs): a structure-function update. *Toxicon X* **7**, 100052
15. Castro, A. C., Escalante, T., Rucavado, A., and Gutiérrez, J. M. (2021) Basement membrane degradation and inflammation play a role in the pulmonary hemorrhage induced by a P-III snake venom metalloproteinase. *Toxicon* **197**, 12–23
16. Gutiérrez, J. M., and Rucavado, A. (2000) Snake venom metalloproteinases: their role in the pathogenesis of local tissue damage. *Biochimie* **82**, 841–850
17. Terra, R. M. S., Pinto, A. F. M., Guimarães, J. A., and Fox, J. W. (2009) Proteomic profiling of snake venom metalloproteinases (SVMPs): insights into venom induced pathology. *Toxicon* **54**, 836–844
18. Gutiérrez, J. M., Escalante, T., Rucavado, A., and Herrera, C. (2016) Hemorrhage caused by snake venom metalloproteinases: a journey of discovery and understanding. *Toxins (Basel).* **8**, 93
19. Brown, N., and Landon, J. (2010) Antivenom: the most cost-effective treatment in the world? *Toxicon* **55**, 1405–1407
20. Agarwal, R., Aggarwal, A. N., Gupta, D., Behera, D., and Jindal, S. K. (2005) Low dose of snake antivenom is as effective as high dose in patients with severe neurotoxic snake envenoming. *Emerg. Med. J.* **22**, 397–399
21. Jones, B. K., Saviola, A. J., Reilly, S. B., Stubbs, A. L., Arida, E., Iskandar, D. T., *et al.* (2019) Venom composition in a Phenotypically variable Pit viper (Trimeresurus insularis) across the lesser Sunda Archipelago. *J. Proteome Res.* **18**, 2206–2220
22. Ciscotto, P. H. C., Rates, B., Silva, D. A. F., Richardson, M., Silva, L. P., Andrade, H., *et al.* (2011) Venomic analysis and evaluation of antivenom cross-reactivity of South American Micrurus species. *J. Proteomics* **74**, 1810–1825
23. Tanaka, G. D., Furtado, M. D. F. D., Portaro, F. C. V., Sant'Anna, O. A., and Tambourgi, D. V. (2010) Diversity of Micrurus snake species related to their venom toxic effects and the prospective of antivenom neutralization. *PLoS Negl. Trop. Dis.* **4**, e622
24. Petras, D., Sanz, L., Segura, Á., Herrera, M., Villalta, M., Solano, D., *et al.* (2011) Snake venomics of African spitting cobras: toxin composition and assessment of congeneric cross-reactivity of the Pan-African EchiTAb-Plus-ICP antivenom by antivenomics and neutralization approaches. *J. Proteome Res.* **10**, 1266–1280
25. Casewell, N. R., Cook, D. A. N., Wagstaff, S. C., Nasidi, A., Durfa, N., Wüster, W., *et al.* (2010) Pre-clinical assays predict Pan-African Echis viper efficacy for a species-specific antivenom. *PLoS Negl. Trop. Dis.* **4**, e851
26. Casewell, N. R., Jackson, T. N. W., Laustsen, A. H., and Sunagar, K. (2020) Causes and consequences of snake venom variation. *Trends Pharmacol. Sci.* **41**, 570–581
27. Saviola, A. J., Pla, D., Sanz, L., Castoe, T. A., Calvete, J. J., and Mackessy, S. P. (2015) Comparative venomics of the Prairie Rattlesnake (*Crotalus viridis viridis*) from Colorado: identification of a novel pattern of ontogenetic changes in venom composition and assessment of the immunoreactivity of the commercial antivenom CroFab®. *J. Proteomics* **121**, 28–43
28. Mackessy, S. P., Williams, K., and Ashton, K. G. (2003) Ontogenetic variation in venom composition and diet of *Crotalus oreganus concolor*. A case of venom paedomorphosis? *Copeia* **2003**, 769–782
29. Cipriani, V., Debono, J., Goldenberg, J., Jackson, T. N. W., Arbuckle, K., Dobson, J., *et al.* (2017) Correlation between ontogenetic dietary shifts and venom variation in Australian brown snakes (Pseudonaja). *Comp. Biochem. Physiol. C Toxicol. Pharmacol.* **197**, 53–60
30. Modahl, C. M., Mukherjee, A. K., and Mackessy, S. P. (2016) An analysis of venom ontogeny and prey-specific toxicity in the monocled cobra (*Naja kaouthia*). *Toxicon* **119**, 8–20
31. Saviola, A. J., Gandara, A. J., Bryson, R. W., and Mackessy, S. P. (2017) Venom phenotypes of the Rock rattlesnake (Crotalus lepidus) and the Ridge-nosed rattlesnake (Crotalus willardi) from México and the United States. *Toxicon* **138**, 119–129

32. Smith, C. F., Nikolakis, Z. L., Ivey, K., Perry, B. W., Schield, D. R., Balchan, N. R., *et al*. (2023) Snakes on a plain: biotic and abiotic factors determine venom compositional variation in a wide-ranging generalist rattlesnake. *BMC Biol.* **21**, 136

33. Senji Laxme, R. R., Attarde, S., Khochare, S., Suranse, V., Martin, G., Casewell, N. R., *et al*. (2021) Biogeographical venom variation in the indian spectacled cobra (Naja naja) underscores the pressing need for pan-India efficacious snakebite therapy. *PLoS Negl. Trop. Dis.* **15**, e0009150

34. Chanda, A., Patra, A., Kalita, B., and Mukherjee, A. K. (2018) Proteomics analysis to compare the venom composition between Naja naja and Naja kaouthia from the same geographical location of eastern India: correlation with pathophysiology of envenomation and immunological cross-reactivity towards commercial polyantiv. *Expert Rev. Proteomics* **15**, 949–961

35. Chanda, A., Kalita, B., Patra, A., Senevirathne, W. D. S. T., and Mukherjee, A. K. (2019) Proteomic analysis and antivenomics study of Western India Naja naja venom: correlation between venom composition and clinical manifestations of cobra bite in this region. *Expert Rev. Proteomics* **16**, 171–184

36. Tan, C. H., Tan, K. Y., Sim, S. M., Fung, S. Y., and Tan, N. H. (2016) Geographical venom variations of the Southeast Asian monocled cobra (Naja kaouthia): venom-induced neuromuscular depression and anti-venom neutralization. *Comp. Biochem. Physiol. C Toxicol. Pharmacol.* **185–186**, 77–86

37. Gutiérrez, J. M., Albulescu, L. O., Clare, R. H., Casewell, N. R., Abd El-Aziz, T. M., Escalante, T., *et al*. (2021) The search for natural and synthetic inhibitors that would complement antivenoms as therapeutics for snakebite envenoming. *Toxins (Basel).* **13**, 451

38. Waiddyanatha, S., Silva, A., Siribaddana, S., and Isbister, G. K. (2019) Long-term effects of snake envenoming. *Toxins (Basel)* **11**, 193

39. Williams, S. S., Wijesinghe, C. A., Jayamanne, S. F., Buckley, N. A., Dawson, A. H., Lalloo, D. G., *et al*. (2011) Delayed psychological morbidity associated with snakebite envenoming. *PLoS Negl. Trop. Dis.* **5**, e1255

40. Rivel, M., Solano, D., Herrera, M., Vargas, M., Villalta, M., Segura, Á., *et al*. (2016) Pathogenesis of dermonecrosis induced by venom of the spitting cobra, Naja nigricollis: an experimental study in mice. *Toxicon* **119**, 171–179

41. Gutiérrez, J. M., León, G., Rojas, G., Lomonte, B., Rucavado, A., and Chaves, F. (1998) Neutralization of local tissue damage induced by Bothrops asper (terciopelo) snake venom. *Toxicon* **36**, 1529–1538

42. Gutiérrez, J. M. (2012) Improving antivenom availability and accessibility: science, technology, and beyond. *Toxicon* **60**, 676–687

43. Gutiérrez, J. M., Williams, D., Fan, H. W., and Warrell, D. A. (2010) Snakebite envenoming from a global perspective: towards an integrated approach. *Toxicon* **56**, 1223–1235

44. De Silva, H. A., Ryan, N. M., and De Silva, H. J. (2016) Adverse reactions to snake antivenom, and their prevention and treatment. *Br. J. Clin. Pharmacol.* **81**, 446–452

45. Fan, H. W., and Monteiro, W. M. (2018) History and perspectives on how to ensure antivenom accessibility in the most remote areas in Brazil. *Toxicon* **151**, 15–23

46. Cristino, J. S., Salazar, G. M., Machado, V. A., Honorato, E., Farias, A. S., Vissoci, J. R. N., *et al*. (2021) A painful journey to antivenom: the therapeutic itinerary of snakebite patients in the Brazilian Amazon (the QUALISnake study). *PLoS Negl. Trop. Dis.* **15**, e0009245

47. Habibid, A. G., Musa, B. M., Iliyasuid, G., Hamza, M., Kuznik, A., and Chippauxid, J. P. (2020) Challenges and prospects of snake antivenom supply in Sub-Saharan Africa. *PLoS Negl. Trop. Dis.* **14**, 1–10

48. Chippaux, J. P. (2011) Estimate of the burden of snakebites in sub-Saharan Africa: a meta-analytic approach. *Toxicon* **57**, 586–599

49. Xie, C., Slagboom, J., Albulescu, L. O., Somsen, G. W., Vonk, F. J., Casewell, N. R., *et al*. (2020) Neutralising effects of small molecule toxin inhibitors on nanofractionated coagulopathic Crotalinae snake venoms. *Acta Pharm. Sin. B* **10**, 1835–1845

50. Albulescu, L. O., Xie, C., Ainsworth, S., Alsolaiss, J., Crittenden, E., Dawson, C. A., *et al*. (2020) A therapeutic combination of two small molecule toxin inhibitors provides broad preclinical efficacy against viper snakebite. *Nat. Commun.* **11**, 6094

51. Layfield, H. J., Williams, H. F., Ravishankar, D., Mehmi, A., Sonavane, M., Salim, A., *et al*. (2020) Repurposing cancer drugs Batimastat and marimastat to Inhibit the activity of a group I metalloprotease from the venom of the western diamondback rattlesnake, Crotalus atrox. *Toxins (Basel)* **12**, 309

52. Fontana Oliveira, I. C., Gutiérrez, J. M., Lewin, M. R., and Oshima-Franco, Y. (2020) Varespladib (LY315920) inhibits neuromuscular blockade induced by Oxyuranus scutellatus venom in a nerve-muscle preparation. *Toxicon* **187**, 101–104

53. Arias, A. S., Rucavado, A., and Gutiérrez, J. M. (2017) Peptidomimetic hydroxamate metalloproteinase inhibitors abrogate local and systemic toxicity induced by Echis ocellatus (saw-scaled) snake venom. *Toxicon* **132**, 40–49

54. Chowdhury, A., Lewin, M. R., Zdenek, C. N., Carter, R., and Fry, B. G. (2021) The relative efficacy of Chemically diverse small-molecule enzyme-inhibitors against anticoagulant activities of African spitting cobra (Naja species) venoms. *Front. Immunol.* **12**, 752442

55. Clare, R. H., Hall, S. R., Patel, R. N., and Casewell, N. R. (2021) Small molecule drug discovery for neglected tropical snakebite. *Trends in Pharmacol. Sci.* **42**, 340–353

56. [preprint] Hall, S. R., Rasmussen, S. A., Crittenden, E., Dawson, C. A., Bartlett, K. E., Westhorpe, A. P., *et al*. (2022) Repurposed drugs and their combinations prevent morbidity-inducing dermonecrosis caused by diverse cytotoxic snake venoms. *bioRxiv*. https://doi.org/10.1101/2022.05.20.492855

57. Gutiérrez, J. M., Lewin, M. R., Williams, D. J., and Lomonte, B. (2020) Varespladib (LY315920) and methyl varespladib (LY333013) abrogate or delay lethality induced by presynaptically acting neurotoxic snake venoms. *Toxins (Basel)* **12**, 131

58. Youngman, N. J., Lewin, M. R., Carter, R., Naude, A., and Fry, B. G. (2022) Efficacy and limitations of Chemically diverse small-molecule enzyme-inhibitors against the Synergistic Coagulotoxic activities of bitis viper venoms. *Molecules* **27**, 1733

59. Lewin, M. R., María Gutiérrez, J., Samuel, S. P., Herrera, M., Bryan-Quirós, W., Lomonte, B., *et al*. (2018) Delayed oral LY333013 rescues mice from highly neurotoxic, lethal doses of papuan taipan (Oxyuranus scutellatus) venom. *Toxins (Basel)* **10**, 380

60. Menzies, S. K., Clare, R. H., Xie, C., Westhorpe, A., Hall, S. R., Edge, R. J., *et al*. (2022) In vitro and in vivo preclinical venom inhibition assays identify metalloproteinase inhibiting drugs as potential future treatments for snakebite envenoming by Dispholidus typus. *Toxicon X* **14**, 100118

61. Xie, C., Albulescu, L. O., Bittenbinder, M. A., Somsen, G. W., Vonk, F. J., Casewell, N. R., *et al*. (2020) Neutralizing effects of small molecule inhibitors and metal chelators on coagulopathic Viperinae snake venom toxins. *Biomedicines* **8**, 297

62. Bittenbinder, M. A., Bergkamp, N. D., Slagboom, J., Bebelman, J. P. M., Casewell, N. R., Siderius, M. H., *et al*. (2023) Monitoring snake venom-induced extracellular matrix degradation and identifying Proteolytically active venom toxins using Fluorescently labeled substrates. *Biology (Basel)*. **12**, 765

63. Evans, J. D., Stark, A., Johnson, C. D., Daniel, F., Carmichael, J., Buckels, J., *et al*. (2001) A phase II trial of marimastat in advanced pancreatic cancer. *Br. J. Cancer* **85**, 1865–1870

64. Quirt, I., Bodurtha, A., Lohmann, R., Rusthoven, J., Belanger, K., Young, V., *et al*. (2002) Phase II study of marimastat (BB-2516) in malignant melanoma: a clinical and tumor biopsy study of the National Cancer Institute of Canada Clinical Trials Group. *Invest. New Drugs* **20**, 431–437

65. Franken, H., Mathieson, T., Childs, D., Sweetman, G. M. A., Werner, T., Tögel, I., *et al*. (2015) Thermal proteome profiling for unbiased identification of direct and indirect drug targets using multiplexed quantitative mass spectrometry. *Nat. Protoc.* **10**, 1567–1593

66. Mateus, A., Kurzawa, N., Becher, I., Sridharan, S., Helm, D., Stein, F., *et al*. (2020) Thermal proteome profiling for interrogating protein interactions. *Mol. Syst. Biol.* **16**, 9232

67. Van Vranken, J. G., Li, J., Mitchell, D. C., Navarrete-Perea, J., and Gygi, S. P. (2021) Assessing target engagement using proteome-wide solvent shift assays. *Elife* **10**, e70784

68. Zhang, X., Wang, Q., Li, Y., Ruan, C., Wang, S., Hu, L., *et al*. (2020) Solvent-induced protein precipitation for drug target discovery on the proteomic scale. *Anal. Chem.* **92**, 1363–1371

69. Mateus, A., Määttä, T. A., and Savitski, M. M. (2017) Thermal proteome profiling: unbiased assessment of protein state through heat-induced stability changes. *Proteome Sci.* **15**, 1–7

70. Gaetani, M., Sabatier, P., Saei, A. A., Beusch, C. M., Yang, Z., Lundström, S. L., *et al.* (2019) Proteome integral solubility alteration: a high-throughput proteomics assay for target deconvolution. *J. Proteome Res.* **18**, 4027–4037

71. Gaetani, M., and Zubarev, R. A. (2023) Proteome integral solubility alteration (PISA) for high-throughput ligand target deconvolution with increased statistical significance and reduced sample amount. *Methods Mol. Biol.* **2554**, 91–106

72. Zhang, X., Lytovchenko, O., Lundström, S., Zubarev, R., and Gaetani, M. (2022) Proteome integral solubility alteration (PISA) assay in Mammalian cells for deep, high-confidence, and high-throughput target deconvolution. *Bio Protoc.* **12**, e4556

73. Lyu, J., Wang, K., and Ye, M. (2020) Modification-free approaches to screen drug targets at proteome level. *TrAC Trends Anal. Chem.* **124**, 115574

74. Zeng, X., Wei, T., Wang, X., Liu, Y., Tan, Z., Zhang, Y., *et al.* (2024) Discovery of metal-binding proteins by thermal proteome profiling. *Nat. Chem. Biol.* https://doi.org/10.1038/s41589-024-01563-y

75. Li, J., Van Vranken, J. G., Paulo, J. A., Huttlin, E. L., and Gygi, S. P. (2020) Selection of heating temperatures improves the sensitivity of the proteome integral solubility alteration assay. *J. Proteome Res.* **19**, 2159–2166

76. Savitski, M. M., Reinhard, F. B. M., Franken, H., Werner, T., Savitski, M. F., Eberhard, D., *et al.* (2014) Tracking cancer drugs in living cells by thermal profiling of the proteome. *Science* **346**, 1255784

77. Mitchell, D. C., Kuljanin, M., Li, J., Van Vranken, J. G., Bulloch, N., Schweppe, D. K., *et al.* (2023) A proteome-wide atlas of drug mechanism of action. *Nat. Biotechnol.* **41**, 845–857

78. Peng, H., Guo, H., Pogoutse, O., Wan, C., Hu, L. Z., Ni, Z., *et al.* (2016) An unbiased chemical proteomics method Identifies FabI as the Primary target of 6-OH-BDE-47. *Environ. Sci. Technol.* **50**, 11329–11336

79. Ruan, C., Ning, W., Liu, Z., Zhang, X., Fang, Z., Li, Y., *et al.* (2022) Precipitate-supported thermal proteome profiling coupled with deep Learning for comprehensive screening of drug target proteins. *ACS Chem. Biol.* **17**, 252–262

80. Modahl, C. M., Mrinalini, F. S., and Mackessy, S. P. (2018) Adaptive evolution of distinct prey-specific toxin genes in rear-fanged snake venom. *Proc. Biol. Sci.* **285**, 20181003

81. Modahl, C. M., Frietze, S., and Mackessy, S. P. (2018) Transcriptome-facilitated proteomic characterization of rear-fanged snake venoms reveal abundant metalloproteinases with enhanced activity. *J. Proteomics* **187**, 223–234

82. Bolger, A. M., Lohse, M., and Usadel, B. (2014) Trimmomatic: a flexible trimmer for Illumina sequence data. *Bioinformatics* **30**, 2114–2120

83. Langmead, B., and Salzberg, S. L. (2012) Fast gapped-read alignment with Bowtie 2. *Nat. Methods* **9**, 357–359

84. Dowell, N. L., Giorgianni, M. W., Kassner, V. A., Selegue, J. E., Sanchez, E. E., and Carroll, S. B. (2016) The deep origin and recent loss of venom toxin genes in rattlesnakes. *Curr. Biol.* **26**, 2434–2445

85. Rokyta, D. R., Lemmon, A. R., Margres, M. J., and Aronow, K. (2012) The venom-gland transcriptome of the eastern diamondback rattlesnake (*Crotalus adamanteus*). *BMC Genomics* **13**, 312

86. McGivern, J. J., Wray, K. P., Margres, M. J., Couch, M. E., Mackessy, S. P., and Rokyta, D. R. (2014) RNA-seq and high-definition mass spectrometry reveal the complex and divergent venoms of two rear-fanged colubrid snakes. *BMC Genomics* **15**, 1–18

87. Zhang, J., Kobert, K., Flouri, T., and Stamatakis, A. (2014) PEAR: a fast and accurate illumina paired-end reAd mergeR. *Bioinformatics* **30**, 614–620

88. Archer, J., Whiteley, G., Casewell, N. R., Harrison, R. A., and Wagstaff, S. C. (2014) VTBuilder: a tool for the assembly of multi isoform transcriptomes. *BMC Bioinformatics* **15**, 389

89. Gilbert, D. G. (2013) Gene-omes built from mRNA-seq not genome DNA. *7th Annual Arthropod Genomics Symposium*. *7th Annual Arthropod Genomics Symposium*. University of Indiana, Blooomington, IN, 47405

90. Li, W., and Godzik, A. (2006) Cd-hit: a fast program for clustering and comparing large sets of protein or nucleotide sequences. *Bioinformatics* **22**, 1658–1659

91. Fu, L., Niu, B., Zhu, Z., Wu, S., and Li, W. (2012) CD-HIT: accelerated for clustering the next-generation sequencing data. *Bioinformatics* **28**, 3150–3152

92. Li, B., and Dewey, C. N. (2011) RSEM: accurate transcript quantification from RNA-Seq data with or without a reference genome. *BMC Bioinformatics* **12**, 323

93. Buchfink, B., Xie, C., and Huson, D. H. (2014) Fast and sensitive protein alignment using DIAMOND. *Nat. Methods* **12**, 59–60

94. Nachtigall, P. G., Rautsaw, R. M., Ellsworth, S. A., Mason, A. J., Rokyta, D. R., Parkinson, C. L., *et al.* (2021) ToxCodAn: a new toxin annotator and guide to venom gland transcriptomics. *Brief. Bioinform.* **22**, bbab095

95. Jarzab, A., Kurzawa, N., Hopf, T., Moerch, M., Zecha, J., Leijten, N., *et al.* (2020) Meltome atlas—thermal proteome stability across the tree of life. *Nat. Methods* **17**, 495–503

96. Smith, C. F., and Mackessy, S. P. (2016) The effects of hybridization on divergent venom phenotypes: characterization of venom from *Crotalus scutulatus scutulatus* × *Crotalus oreganus helleri* hybrids. *Toxicon* **120**, 110–123

97. Calvete, J. J., Fasoli, E., Sanz, L., Boschetti, E., and Righetti, P. G. (2009) Exploring the venom proteome of the western diamondback rattlesnake, Crotalus atrox, via snake venomics and combinatorial peptide ligand library approaches. *J. Proteome Res.* **8**, 3055–3067

98. Mackessy, S. P. (2008) Venom composition in rattlesnakes: trends and biological significance. In: *The Biology of Rattlesnakes*. Loma Linda University Press, Loma Linda

99. The field of Reptile toxinology: snakes, Lizards, and their venoms. (2020) In: *Handbook of Venoms and Toxins of Reptiles*. CRC Press Bacon Raton, FL

100. Dzieciatkowska, M., Hill, R., and Hansen, K. C. (2014) GeLC-MS/MS analysis of complex protein mixtures. *Methods Mol. Biol.* **1156**, 53–66

101. Yu, F., Teo, G. C., Kong, A. T., Haynes, S. E., Avtonomov, D. M., Geiszler, D. J., *et al.* (2020) Identification of modified peptides using localization-aware open search. *Nat. Commun.* **11**, 1–9

102. Kong, A. T., Leprevost, F. V., Avtonomov, D. M., Mellacheruvu, D., and Nesvizhskii, A. I. (2017) MSFragger: ultrafast and comprehensive peptide identification in mass spectrometry-based proteomics. *Nat. Methods* **14**, 513–520

103. Zhu, W., Smith, J. W., and Huang, C. M. (2010) Mass spectrometry-based label-free quantitative proteomics. *J. Biomed. Biotechnol.* **2010**, 840518

104. Ji, H., Lu, X., Zheng, Z., Sun, S., and Tan, C. S. H. (2022) ProSAP: a GUI software tool for statistical analysis and assessment of thermal stability data. *Brief. Bioinform.* **23**, bbac057

105. Giorgianni, M. W., Dowell, N. L., Griffin, S., Kassner, V. A., Selegue, J. E., and Carroll, S. B. (2020) The origin and diversification of a novel protein family in venomous snakes. *Proc. Natl. Acad. Sci. U. S. A.* **117**, 10911–10920

106. Harrison, R. A., Oluoch, G. O., Ainsworth, S., Alsolaiss, J., Bolton, F., Arias, A. S., *et al.* (2017) Preclinical antivenom-efficacy testing reveals potentially disturbing deficiencies of snakebite treatment capability in East Africa. *PLoS Negl. Trop. Dis.* **11**, e0005969

107. Lewin, M. R., Carter, R. W., Matteo, I. A., Samuel, S. P., Rao, S., Fry, B. G., *et al.* (2022) Varespladib in the treatment of snakebite envenoming: development history and preclinical evidence supporting Advancement to clinical trials in patients Bitten by venomous snakes. *Toxins (Basel)* **14**, 783

108. Abouyannis, M., FitzGerald, R., Ngama, M., Mwangudzah, H., Nyambura, Y. K., Ngome, S., *et al.* (2022) TRUE-1: trial of Repurposed Unithiol for snakebite Envenoming phase 1 (safety, tolerability, pharmacokinetics and pharmacodynamics in healthy Kenyan adults). *Wellcome Open Res.* **7**, 90

109. Lewin, M., Samuel, S., Merkel, J., and Bickler, P. (2016) Varespladib (LY315920) appears to be a potent, broad-spectrum, inhibitor of snake venom phospholipase A2 and a possible pre-referral treatment for envenomation. *Toxins (Basel)* **8**, 248

110. Bryan-Quirós, W., Fernández, J., Gutiérrez, J. M., Lewin, M. R., and Lomonte, B. (2019) Neutralizing properties of LY315920 toward snake venom group I and II myotoxic phospholipases A2. *Toxicon* **157**, 1–7

111. Xie, C., Albulescu, L. O., Still, K. B. M., Slagboom, J., Zhao, Y., Jiang, Z., *et al.* (2020) Varespladib inhibits the phospholipase A2 and coagulopathic activities of venom components from hemotoxic snakes. *Biomedicines* **8**, 1–17

112. Youngman, N. J., Walker, A., Naude, A., Coster, K., Sundman, E., and Fry, B. G. (2020) Varespladib (LY315920) neutralises phospholipase A2

mediated prothrombinase-inhibition induced by Bitis snake venoms. *Comp. Biochem. Physiol. Toxicol. Pharmacol.* **236**, 108818

113. Dashevsky, D., Bénard-Valle, M., Neri-Castro, E., Youngman, N. J., Zdenek, C. N., Alagón, A., *et al.* (2021) Anticoagulant Micrurus venoms: targets and neutralization. *Toxicol Lett.* **337**, 91–97

114. Molina, D. M., Jafari, R., Ignatushchenko, M., Seki, T., Larsson, E. A., Dan, C., *et al.* (2013) Monitoring drug target engagement in cells and tissues using the cellular thermal shift assay. *Science* **341**, 84–87

115. Albulescu, L. O., Hale, M. S., Ainsworth, S., Alsolaiss, J., Crittenden, E., Calvete, J. J., *et al.* (2020) Preclinical validation of a repurposed metal chelator as an early-intervention therapeutic for hemotoxic snakebite. *Sci. Transl. Med.* **12**, eaay8314

116. Lewis, R. J., and Garcia, M. L. (2003) Therapeutic potential of venom peptides. *Nat. Rev. Drug Discov.* **2**, 790–802

117. García-Fandiño, R., Bernadó, P., Ayuso-Tejedor, S., Sancho, J., and Orozco, M. (2012) Defining the Nature of thermal intermediate in 3 state folding proteins: apoflavodoxin, a study case. *PLoS Comput. Biol.* **8**, e1002647

118. Tang, R., Gasvoda, K. L., Rabin, J., and Alsberg, E. (2023) Protein conformation stabilized by newly formed turns for thermal resilience. *Biophys. J.* **122**, 82–89

119. Panecka-Hofman, J., Pöhner, I., Spyrakis, F., Zeppelin, T., Di Pisa, F., Dello Iacono, L., *et al.* (2017) Comparative mapping of on-targets and off-targets for the discovery of anti-trypanosomatid folate pathway inhibitors. *Biochim. Biophys. Acta Gen. Subj.* **1861**, 3215–3230

120. Dwivedi, A. K., Gurjar, V., Kumar, S., and Singh, N. (2015) Molecular basis for nonspecificity of nonsteroidal anti-inflammatory drugs (NSAIDs). *Drug Discov. Today* **20**, 863–873

121. Doley, R., and Kini, R. M. (2009) Protein complexes in snake venom. *Cell. Mol. Life Sci.* **66**, 2851–2871

122. Montecucco, C., Gutiérrez, J. M., and Lomonte, B. (2008) Cellular pathology induced by snake venom phospholipase A2 myotoxins and neurotoxins: common aspects of their mechanisms of action. *Cell. Mol. Life Sci.* **65**, 2897–2912

123. Shashidharamurthy, R., and Kemparaju, K. (2006) A neurotoxic phospholipase A2 variant: isolation and characterization from eastern regional Indian cobra (Naja naja) venom. *Toxicon* **47**, 727–733

124. Xiao, H., Li, H., Zhang, D., Li, Y., Sun, S., and Huang, C. (2018) Inactivation of venom PLA2 alleviates myonecrosis and facilitates muscle regeneration in envenomed mice: a time course observation. *Molecules* **23**, 1911

125. Moura-da-Silva, A. M., Almeida, M. T., Portes-Junior, J. A., Nicolau, C. A., Gomes-Neto, F., and Valente, R. H. (2016) Processing of snake venom metalloproteinases: generation of toxin diversity and enzyme inactivation. *Toxins (Basel)* **8**, 183

126. Deshimaru, M., Ogawa, T., Nakashima, K., Nobuhisa, I., Chijiwa, T., Shimohigashi, Y., *et al.* (1996) Accelerated evolution of crotalinae snake venom gland serine proteases. *FEBS Lett.* **397**, 83–88

127. Kini, R. M., and Chan, Y. M. (1999) Accelerated evolution and molecular surface of venom phospholipase A2 enzymes. *J Mol Evol* **48**, 125–132

128. Lynch, V. J. (2007) Inventing an arsenal: adaptive evolution and neofunctionalization of snake venom phospholipase A2 genes. *BMC Evol. Biol.* **7**, 2

129. Kini, R. M. (2011) Evolution of three-finger toxins - a versatile mini protein scaffold. *Acta Chim. Slov.* **58**, 693–701

130. Sunagar, K., Fry, B. G., Jackson, T. N. W., Casewell, N. R., Undheim, E. A. B., Vidal, N., *et al.* (2013) Molecular evolution of vertebrate neurotrophins: co-option of the highly conserved nerve growth factor gene into the advanced snake venom arsenalf. *PLoS One* **8**, e81827

131. Lomonte, B., and Calvete, J. J. (2017) Strategies in 'snake venomics' aiming at an integrative view of compositional, functional, and immunological characteristics of venoms. *J. Venom. Anim. Toxins Incl. Trop. Dis.* **23**, 26

132. Slagboom, J., Kaal, C., Arrahman, A., Vonk, F. J., Somsen, G. W., Calvete, J. J., *et al.* (2022) Analytical strategies in venomics. *Microchem. J.* **175**, 107187

133. Lauridsen, L. P., Laustsen, A. H., Lomonte, B., and Gutiérrez, J. M. (2017) Exploring the venom of the forest cobra snake: toxicovenomics and antivenom profiling of Naja melanoleuca. *J. Proteomics* **150**, 98–108

134. Calvete, J. J., Lomonte, B., Saviola, A. J., Bonilla, F., Sasa, M., Williams, D. J., *et al.* (2021) Mutual enlightenment: a toolbox of concepts and methods for integrating evolutionary and clinical toxinology via snake venomics and the contextual stance. *Toxicon X* **9–10**, 100070